UNIVERSITY OF CALIFORNIA
RIVERSIDE

Characterization of Late Holocene Sediment Deposition in the Barrier Estuary of a Small, Mountainous Coastal Watershed

A Thesis submitted in partial satisfaction
of the requirements for the degree of

Master of Science

in

Environmental Sciences

by

Julianna E. McDonnell

December 2019

Thesis Committee:

Dr. Andrew Gray, Chairperson
Dr. James Sickman
Dr. Laosheng Wu

The Thesis of Julianna E. McDonnell is approved by:

_____

_____

_____
Committee Chairperson

University of California, Riverside

Table of Contents

List of Figures

List of Tables

Introduction

Coastal estuaries and lagoons are an important dynamic transitional zone between the terrestrial and marine realms. These environments are heavily influenced by the terrestrial processes within the watershed, regional and global climate forcings, and marine processes over event to millennial time scales (Flemming, 2011). As some of the most productive environments in the world (Camacho-Valdez *et al.*, 2013), coastal estuaries are vital habitat for numerous species of birds, fish, and other aquatic organisms, and provide a wealth of ecosystem services such as the reduction of nutrient loads and carbon sequestration (Nelleman *et al.*, 2009). They also act as buffers that protect coastal habitats and human infrastructure during storm events by dissipating wave energy and reducing storm surges (Costanza *et al.*, 2008; Mudd *et al.*, 2009; Nelleman *et al.*, 2009).

Estuaries are also where marine processing of terrestrial sediments begins, and thus play a significant role in global sediment dynamics. They receive watershed sediments delivered from the estuary's associated fluvial system(s), and marine sediments from littoral cells. The marine sediments are derived from the nearshore zone and wave driven coastal erosion during severe storm events (Best & Griggs, 1991; Perg *et al.*, 2003). The delivery of sediment from the littoral cell to a coastal estuary fluctuates, depending on storm frequency, tidal conditions, geologic type of estuary, etc. Of course, the magnitude and timing of terrestrial sediment delivery from the watershed also varies, responding to external changes in climate and tectonism, as well as internal changes to the watershed such as land cover and land use that influence both sediment source and transport to the estuary. Most estuaries have been around for thousands of years, storing sediment as a

function of accommodation space developed by rising relative sea level (Levinton, 1995; McBride *et al.*, 2013). Because of this, sediments deposited in an estuary can serve as an archive of geomorphic change often extending back for millennia, as well as a record of watershed and marine responses to climatic and human related disturbances.

Particle size distributions are a fundamental metric used by sedimentologists to deduce meaningful information from sediment deposits regarding source, transporting agent, and/or depositional environment (Chambers & Upchurch, 1979; Tanner, 1991, 1995; Poizot *et al.*, 2008). Sediments are derived from multiple sources with their own textural attributes that have experienced various erosional processes and transport mechanisms, which selectively remove certain size classes and alter the particle size distribution of the remaining sediment (Yu & Oldfield, 1989). Depositional environments are assumed to have their own characteristic energy conditions resulting in specific textural attributes, but the particle size distributions of deposited sediments often reflect the selective energy of the transporting agent as well (Sahu, 1964; Chambers & Upchurch, 1979).

Particle size distributions can reveal a lot about the transporting agent. First, a few terms should be defined. Particle diameters are either typically expressed in SI units (μm or mm), or units of phi (φ). Phi is calculated by the equation $-\log_2(D/D_0)$, where D refers to particle diameter in mm, and D_0 refers to a reference diameter of 1 mm (Krumbein, 1934). In some cases, portions of the particle size distribution can be attributed to particular transport mechanisms. For example, in the context of fluvial transport, particles between 0.5 to 3 φ mark a transition zone between surface creep along the channel bed and

suspension in the water column (Visher, 1969), with the boundary between the two around 2 φ, depending on specific flow field energetics (Bagnold, 1966). Skewness, a measure of asymmetry or the degree to which a curve "skews" from a symmetrical normal distribution, is a commonly used value to categorize particle size distributions (Folk & Ward, 1957; Friedman, 1961; Valia & Cameron, 1977). Positive skewness, referring to a particle size distribution in which the mode is skewed towards more positive values in φ space, or smaller particle sizes, is often a result of unidirectional flow via water or wind. This is because the capacity to transport fine particles does not vary as greatly as the transport of larger particles (Martins, 1965). Negative skewness occurs when winnowing action effectively removes the fine fraction of the curve. This is caused by velocity fluctuations in higher energy depositing agents, the addition of coarse material like shell fragments, or because the sediments were in transport for a long period of time (Sahu, 1964; Martins, 1965). For example, beach sands almost always have negative skewness while river sands generally have positive skewness (Tanner, 1995).

Another common approach is plotting two particle size statistical parameters against one another (i.e. mean particle size vs. standard deviation, skewness vs. kurtosis) as a bivariate diagram (Friedman, 1961; Moiola & Weiser, 1968; Friedman & Sanders, 1978; Tanner, 1991; Lario *et al.*, 2002). Different transporting agents/depositional environments tend to plot in distinct zones of the bivariate space, which provides an opportunity to identify and discern information about older sediment deposits. Ternary plots can also be useful for inference of hydrodynamic conditions during deposition, as increasing clay content indicates lower energy conditions (Pejrup, 1988; Flemming, 2000).

Plots like these can be informative when trying to reconstruct past depositional conditions, but have typically been found to be most effective when combined with other lines of sedimentological evidence (Watson *et al.*, 2013; Gray *et al.*, 2016; Oczkowski *et al.*, 2019).

While the characterization of sediment particle size distributions is often used for historical analysis of the geomorphic behavior of depositional settings, the potential mosaic of source, transport, and depositional properties can complicate interpretation. Chambers and Upchurch (1971) compared sediments from two different depositional environments and found that the particle size distributions did not always reflect the depositional environment from which the sediment was collected. They found that sediments with more narrow size ranges (i.e. sediments from littoral cell, sand dunes, etc.) have less flexibility to express the changes wrought by subsequent energetic processes (Chambers & Upchurch, 1979). In order to distinguish between these processes, multiproxy studies have become the norm (Stewart, 1958; Szczuciński *et al.*, 2012; Watson *et al.*, 2013; Clarke *et al.*, 2014; Gray *et al.*, 2016). For example, marine diatoms and nannoliths can be paired with particle size data to identify paleotsunami deposits (Hemphill-Haley, 1996; Szczuciński *et al.*, 2012). Watson et al. (2013) paired sediment textural parameters and bivariate plots with sedimentary organic matter stable isotope analyses, pollen analysis, and historical imagery to identify a mid-twentieth century shift in the structure and function of a coastal lagoon in California. Clarke (2014) used high resolution particle size data to perform end member analysis and coupled it with core chronological evidence and X-ray fluorescence data to reconstruct barrier conditions in a back-barrier lagoon at annual to centennial time scales. Also, Gray et al. (2016) reconstructed planform geomorphic change from sequences of

aerial photographs and paired it with high resolution particle size data to identify the stratigraphic signature of channel meander abandonment sequences in a tidal estuary. These examples illustrate that paleoenvironmental reconstruction studies typically require a multifaceted approach, often connecting multiple particle size parameters with other lines of evidence to understand sedimentary processes at play in complex depositional environments.

The goal of this study was to investigate and reconstruct the geomorphic history of Scott Creek Estuary and Lagoon, a coastal estuary in central California, over the last two millennia (see Fig. 1 for location). The focus of this work was to better understand both the natural sedimentological functioning of the estuary and the effects of major human alteration in the last century. Extensive previous work had developed a baseline understanding of the ecohydrology of the estuarine marsh system (Environmental Science Associates, 2017), but fundamental gaps remained, particularly regarding the processes governing sediment deposition in the marsh and the behavior of the system prior to extensive human intervention in the early twentieth century.

Like most of the small mountainous rivers draining the Pacific West Coast of the US, the mouth of Scott Creek is often impounded by wave-built sand bars, creating a freshwater lagoon system that can persist for months before breaching, potentially influencing sediment accumulation rates. As part of highway development in the late 1930s, the lower reaches of Scott Creek were modified and relocated to fix its outlet under a newly constructed bridge (ESA, 2017). The behavior of lower Scott Creek and sedimentation patterns within the estuary prior to these dramatic human modifications is

not well understood. These modifications most likely altered the sediment connectivity between Scott Creek and its marsh, influencing the sediment trapping efficiency of the estuary and feedback mechanisms associated with the episodic nature of sediment delivery and deposition in these types of systems.

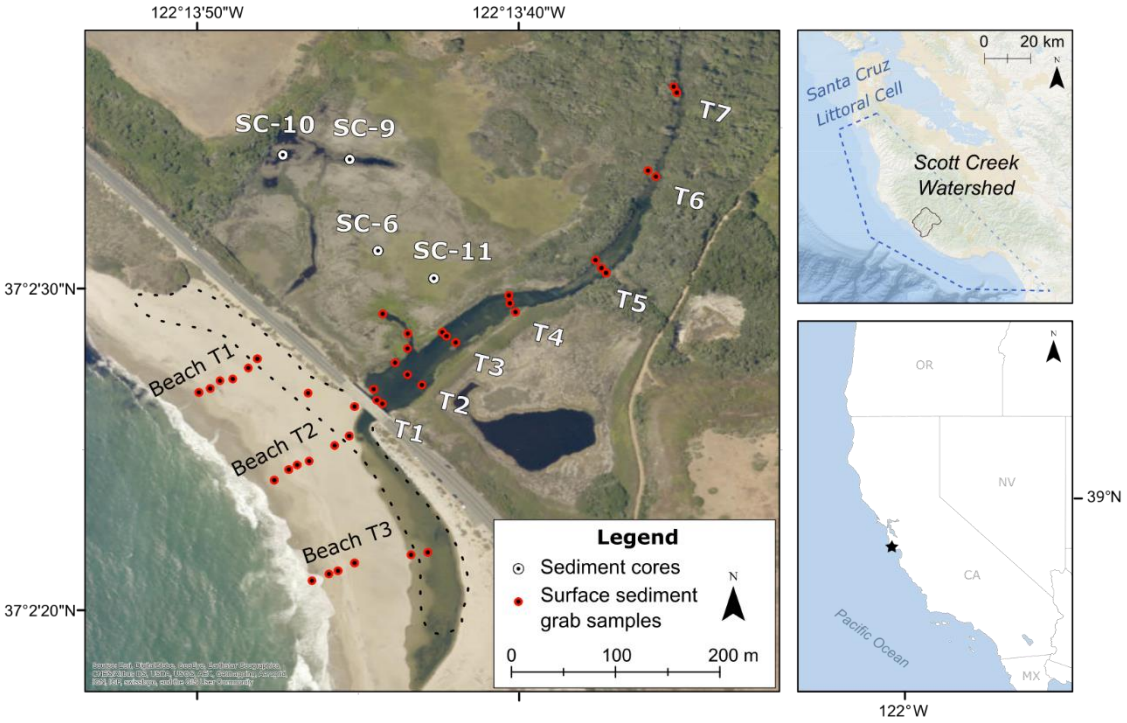

Fig. 1. Location of Scott Creek Estuary. Dashed black line indicates the location of the flooded channel along the beach at the time of sample collection (May 2019).

This work was motivated by the fundamental question: what did this system look like prior to these anthropogenic changes? How did Scott Creek behave once it reached the estuary, and how connected was the channel to the marsh? These questions were addressed using a multifaceted approach to identify depositional changes in the last 2,000 years, including active and abandoned channel sequences, periods of barrier closure, and storm events. Additionally, sedimentation rates were quantified over the time period directly before and after the hydrological modifications to lower Scott Creek (i.e. the last few to

several hundred years of deposition). These analyses were used to disentangle lagoon sediment dynamics, both natural and after extensive hydro-modification, as well as the history of sediment delivery to the marsh platform. This will inform the understanding and prediction of the future accretionary trajectory of Scott Creek Estuary in the context of rising sea level associated with a changing climate.

Methods

This study was performed by collecting and analyzing sediment cores from different environments within the North Marsh of the Scott Creek Estuary, and surface sediment samples from Scott Creek channel and beach. Chronological models were produced for multiple cores using fallout radionuclides (Pb-210 and Cs-137) and radiocarbon. Marsh and channel geomorphology were reconstructed over the last 2,000 years by identifying diagnostic characteristics in the particle size distributions of the marsh cores. These sediments were categorized into different depositional environments using bivariate domains dictated by descriptive statistics, end member modelling, and reference sediments from known depositional environments (current beach and channel sediment samples, or older sediments whose depositional environments were approximated using historical aerial imagery). To assess the recent depositional history of the marsh in the last 150 years, sedimentation rates were estimated on the basis of stratigraphic evidence and fallout radionuclide activity, and considered in the context of historical human activities in the lagoon and watershed, as well as documented changes in the planform geomorphology

of the estuary through aerial photographs and topographic maps produced between 1853 and 1940.

Study Region

Scott Creek is a small, 19.6 km long coastal stream draining 77 km^2 of the Santa Cruz Mountains in the central California Coast Ranges in Santa Cruz County (Fig. 1). The watershed is mostly composed of Cretaceous granitic rocks and Paleozoic metamorphics (marbles and schists). This basement complex is overlain by Tertiary marine sedimentary units, namely the Upper Miocene to Pliocene Santa Cruz Mudstone and Purisima Formation near Scott Creek. Multiple marine terraces carve the landscape, which are capped by a thin layer (1.5-6 m) of paleobeach and marine sediments (Clark, 1981; Best & Griggs, 1991; Perg *et al.*, 2003). The Tertiary bedrock is covered by a thin veneer of colluvium and soil, and there is very little sediment storage in the upper watershed (Best & Griggs, 1991). The surrounding sea cliffs (5-30 m high) are punctuated by a small pocket beach that was carved by Scott Creek, forming a coastal lagoon as it was drowned by Holocene sea level rise (Best & Griggs, 1991; ESA, 2001). Sediment input to the lagoon system is either fluvially derived from the watershed, or marine derived from the Santa Cruz littoral cell. Five major fluvial systems account for 75-90% of the sediment inputs to the littoral cell, and the rest comes from cliff back-wearing of the terrace deposits or sand dune deflation (Perg *et al.*, 2003). Finer grained sediment is transported offshore, while coarser grained material remains in the littoral cell (Santa Cruz cell cutoff diameter is 0.18

mm) until being deposited in any of the pocket beaches within the cell, or until it reaches the Monterey Submarine Canyon (Best & Griggs, 1991).

There is proof of native inhabitants living in the area as far back as 5000 BCE (Jones & Hildebrandt, 1988). During the mission period (1770-1835 CE), the subsistence-based lifestyle of the native Costanoan people was replaced by agriculture, namely livestock production (Levy, 1977). Livestock production and dairying continued to be the most prominent land use in the area until the late nineteenth century, when more intensive crop farming and commercial logging efforts flourished with the construction of railroads (ESA, 2001). Intense periods of logging occurred between 1906 and 1920, and 1940 to 1960 (ESA & SWCA Environmental Consultants, 2012), but both farming and logging efforts started to decline in the 1970s. Currently, the watershed is 95% privately owned and is still used for agriculture and timber harvesting, as well as rural residential housing and recreation (ESA, 2001).

The Scott Creek watershed belongs in a Mediterranean climate, receiving most of its precipitation (annual average of 100 cm) during intense winter storm events (Grantham *et al.*, 2010; Clarke *et al.*, 2014). A USGS streamflow gage infrequently monitored Scott Creek between 1937 and 1982, but the gage location was upstream of a tributary confluence (ESA & SWCA, 2012). In general, peak discharge in the winter is highly episodic and variable, but can easily exceed 65 $m^3 \cdot s^{-1}$ (Osterback *et al.*, 2018). The summers have almost no rainfall and very low base flow in the channel (<0.1 $m^3 \cdot s^{-1}$), resulting in closure of the sand bar barrier and eventual filling of the back-barrier marsh to create a freshwater lagoon. Barrier closure can persist for months, opening in late fall or winter when higher

energy waves and increased precipitation allow streamflow to surpass the level of the sand bar (Smith, 1990; Nylen, 2015; ESA, 2017). The barrier opening is usually perched above oceanic tides so there is very little tidal interaction with the channel and marsh (ESA, 2017).

In the 1930s, the meandering channel was straightened and relocated under the new bridge (completed in 1938) using artificial levees, training berms, and causeways, altering many hydrogeomorphic functions of lower Scott Creek, including a decrease in connectivity between the channel and its lagoon and marsh (Fig. 2). Large winter storms associated with El Niño years typically result in flood conditions that can overcome these modifications, with the largest flood event occurring in 1955. This event caused the channel to breach its artificial levees and deposited a thick package of sediment on the marsh (i.e. a crevasse splay).

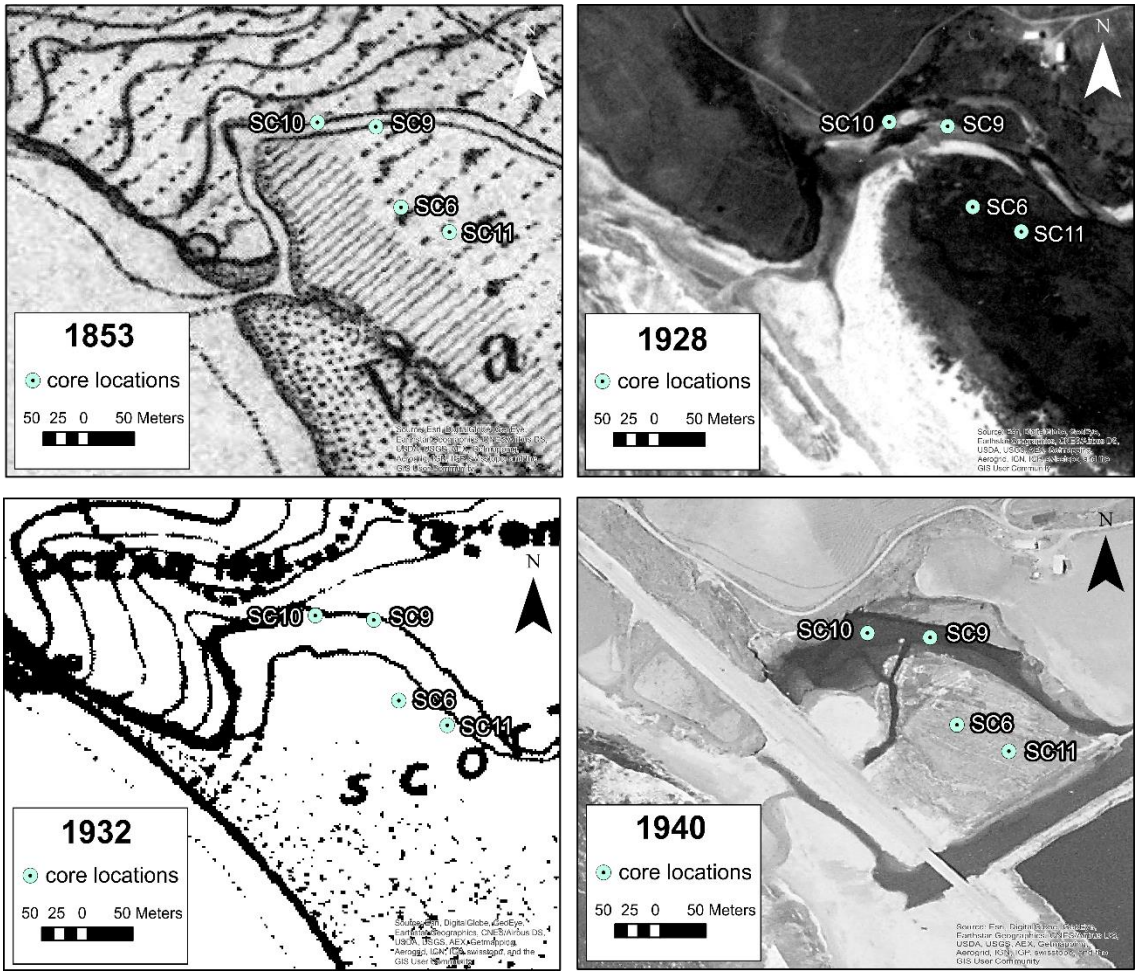

Fig. 2. Location of Lower Scott Creek prior to bridge emplacement (1853-1932 images) and post-bridge emplacement (1940 image). Shoreline topographic maps provided by United States National Geodetic Survey. 1928 aerial image acquired from University of California, Santa Cruz, 1940 image from University of California, Santa Barbara

Sediment Sample Collection

Two methods of sediment core collection were used. Shallow cores (20-40 cm depth) were collected from the North Marsh using a hand and slide-hammer driven Russian Peat Borer during a preliminary site visit under flooded marsh conditions. These cores were used only to confirm that fallout radionuclide approaches were appropriate for dating sediment deposits at the study site (results not shown). On a subsequent site visit under drained marsh conditions on March 3rd-4th, 2018, two cores were collected from the North Marsh platform and two from a relic Scott Creek channel with a vibracoring device driving 7.6 cm diameter aluminum irrigation pipe. Recovered core depths ranged from 88 to 317.5 cm (Table 1). Coring in the relic channel (SC-9 and SC-10) was challenging due to unconsolidated sediments, resulting in relatively short recovery lengths (88 to 123 cm). However, the two longer cores recovered from the marsh platform, core SC-6 (317.5 cm) and core SC-11 (269 cm), provided records that spanned the period of interest.

Table 1. Core details

Location	Landform	ID #	Latitude*	Longitude*	Depth (cm)	Date of collection
Scott Creek	Marsh Platform	SC-6	37.041995°	-122.228993°	317.5	3/3/2018
Scott Creek	Relic Channel	SC-9	37.042782°	-122.229238°	123	3/4/2018
Scott Creek	Relic Channel	SC-10	37.042823°	-122.229817°	88	3/4/2018
Scott Creek	Marsh Platform	SC-11	37.041755°	-122.228512°	269	3/4/2018

***** Datum: WGS 1984 EPSG:4326

Surface sediment samples were collected on May 14th-15th, 2019 from the beach and lower Scott Creek. Surface sediment samples (upper 2-3 cm) were collected from the beach in three transects (SCBT1, T2, T3) during low tide conditions. The transects consisted of six different points along the beach profile: the nearshore zone (NS), two from

the foreshore (FS1 and FS2), the top of the berm (B), behind the berm (BB), and from the flooded beach channel running parallel to the shore (ASC). Three subsamples were collected from a 1 m^2 grid for each point of the transect using a small trowel. Additionally, surface sediment samples were collected from seven transects spaced 30 - 100 m apart along the lower Scott Creek channel, with transect 1 (SCCT1) starting just upstream of the bridge. Three samples were collected across each transect with a ponar mini grab sampler: from the estimated thalweg (T1_TH, for example), and a quarter of the distance from either berm (N and S, or middle, if the thalweg was closer to one bank). Samples within transects 6 and 7 were combined as the coarse sediments required a much larger population for representative sieve fractions. Three grab samples were also collected from the lateral "finger" channel between T2 and T3.

Stratigraphic Description and Physical Characterization

After collection, the cores were transported to UCR for analysis and stored under refrigeration. All cores were split, described, and subsampled for physical and chronological analyses. Preliminary stratigraphic descriptions included notation of color, bedding structure, texture, and the presence of roots and organic material down core. Stratigraphic information was entered into PSICAT 1.0.0 for visualization.

Subsamples were collected for bulk density and particle size distribution analyses on the basis of stratigraphic changes. Dry bulk density was estimated by dividing sediment subsample dry mass by volume. Subsamples were collected using a fixed volume, dried at 105°C for 24 hours, and weighted on a 5-place balance after cooling under vacuum

desiccation to obtain dry mass. Particle size distribution analyses were run for each stratigraphic unit identified in each of the two longer cores. All fine particle size samples (maximum diameter (D) < 2 mm) were pre-treated according to Gray *et al.* (2010) and run on a Beckman Coulter LS-13-320 laser diffraction particle size analyzer. Samples with D > 2 mm were characterized using both the laser particle size analyzer and a wet nested sieving technique (see Gray *et al*., 2016). These data were then analyzed by GRADISTAT v.8, a Microsoft Excel based program that reports sediment texture classes and other descriptive particle size statistics on the basis of the full method of moments, with texture classes defined as follows: clay (D < 2 μm), silt (2 μm ≤ D < 63 μm), sand (63 μm ≤ D < 2 mm), and gravel (2 mm ≤ D < 64 mm) (Blott & Pye, 2001). Descriptive terminology for the texture classes of stratigraphic intervals were classified as per Folk (1954).

Fallout Radionuclide (Cs-137 and excess Pb-210) Analysis

Sediment subsamples for fallout radionuclide analysis were collected from the two long cores (SC-6 and SC-11) and one shorter core collected from the channel location prior to bridge emplacement (SC-9) at 1 cm intervals from 0-10 cm depths, 2 cm intervals from 10-30 cm depths, and every 10cm from 30-70 cm depths. Subsequent analysis was required for the 30-70 cm sections of SC-9 and SC-11 at 2 cm intervals. Each sampled horizon was homogenized in a plastic sample bag and then subsampled to obtain at least 6 cc of sediment. Subsamples were then dried at 105 °C for 24 hours, lightly crushed to break up aggregates, and then 3.4 cc volumes were loaded in vials, weighed and sealed with epoxy for a minimum of 21 days before analysis to achieve secular equilibrium between Ra-226

and Rn-222. Gamma spectra were then counted on a Canberra GSW120 SAGe high purity germanium multichannel well detector for a minimum of 80,000 seconds. Activities for Cs-137, total Pb-210, and Pb-214 were estimated using Canberra Genie 2000 software calibrated with geometric standards obtained from Eckert and Ziegler. Excess Pb-210 (Pb-210ex), was estimated by subtracting Pb-214 activity from total Pb-210 activity (see the Chronological Models section for more details).

Radiocarbon Analysis

Roots from the top of peaty horizons and seeds were used for radiocarbon dating in collaboration with the W. M. Keck Carbon Cycle Accelerator Mass Spectrometry Laboratory at the University of California, Irvine. Samples were pre-treated with acid (HCl), followed by repeated base washes (NaOH) and a final HCl acid wash. Pre-treated samples were then converted to carbon dioxide via combustion and reduced to graphite before AMS analysis. Radiocarbon dates were calibrated via Calib using the IntCal 13 calibration curve, and Calibomb for modern dates using the Northern Hemisphere Zone 2 (NH2) calibration dataset (Reimer *et al.*, 2013).

Chronological Models

Chronological models were developed for cores SC-6, SC-9, and SC-11. Recent (age < ~ 100 yrs) sediment deposits were dated using a combination of stratigraphic markers, radioactive isotope fallout (Cs-137) and enrichment (C-14) from above ground nuclear testing, and Pb-210ex inventories. The levee breach on lower Scott Creek during the 1955 flood resulted in a documented crevasse-splay deposit of sufficient depth to effect

vegetation changes (high marsh or upland) on interior portions of the North Marsh (ESA, 2017). The potential for massive deposits poor in organic material and fallout radionuclides from this event were included in our chronological interpretations. When creating the age models for SC-6 and SC-11, this abrupt sedimentation event was identified and omitted, but the top of the deposit was used as a stratigraphic age marker. Sediment deposits older than ~ 100 years were dated with radiocarbon techniques alone.

Above ground nuclear testing introduced Cs-137 and effectively doubled the amount of C-14 in the Earth's atmosphere, mostly during the 1950s and 1960s (Rafter & Fergusson, 1957). Radiocesium appears in North American sediment record starting in 1954. As bomb testing continued, Cs-137 deposition increased until 1963, when the Partial Nuclear Test Bomb Treaty was put in place (Waters *et al.*, 2015). Although both Cs-137 onset (1954) and peak activity (1963) have been employed to date sediment deposits, we have only used the latter because of higher confidence in peak assignment. A constant rate of supply (CRS) model was used to estimate sediment chronologies on the basis of excess Pb-210ex, the fraction of Pb-210 in a given sediment deposit that is not 'supported' by in-situ production from the U-238 decay chain. In the CRS model Pb-210ex is assumed to be entirely delivered as fallout from the atmosphere at a constant rate, but sedimentation rates are allowed to vary (Appleby & Oldfield, 1978). Carbon dates were used after calibration through methods cited in the Radiocarbon Analysis section. Reliable dates were analyzed in Bacon, an age-depth modeling software implemented in R (Blaauw & Christen, 2011). This model divides each core into separate sections, estimates accumulation rates within

those sections using millions of Markov Chain Monte Carlo iterations, and forms an age-depth model using the estimated accumulation rates.

Particle Size Distribution Analysis

In order to estimate possible particle size end members, particle size distributions were fed into an R package called EMMAgeo (Dietze *et al.*, 2012; Dietze & Dietze, 2019). This R package is based on EMMA MATLAB code (Dietze *et al.*, 2012), which derives statistically meaningful particle size end members and quantifies relative contribution of endmembers in individual samples. This is done through eigenspace analysis in combination with scaling procedures and multivariate methods to describe the data set as a linear combination of end member loadings, end member scores and the associated error matrix. See source papers for details on analysis.

A complementary analysis of particle size distribution types was also performed manually. Particle size distributions from marsh sediments were organized into 5 distinct groups based on general shape and location of modes. These were then plotted in bivariate space (mean diameter vs standard deviation or sorting, sorting vs. skewness, etc.) to identify different depositional environments or sources of sediment (Friedman, 1961; Moiola & Weiser, 1968; Tanner, 1991). The channel and beach sediment samples were used for comparison. Aerial imagery from 1928 and shoreline topographic maps made by the United States National Geodetic Survey (formerly U.S. Coast Survey, then U.S. Coast and Geodetic Survey) from 1853 and 1932 were used to verify that cores SC-9 and SC-10 were located in Scott Creek channel prior to its relocation around 1938 (see Fig. 2).

Sedimentation and Sediment Accumulation Rates

Average sedimentation rates (depth/time) were calculated between dated intervals from the Bacon age model. Lower-bound and upper-bound estimates were calculated using maximum and minimum ages (on the basis of 2σ date confidence intervals) for any given depth interval. Average sediment accumulation rates (units of g cm^{-2} yr^{-1}) were calculated for the same intervals to test if any sedimentation rate trends were the result of compaction or compositional changes downcore.

Sedimentation rates were calculated for a range of depth/time intervals, in an attempt to capture both long term trends and the more detailed variability within the longer intervals. Though an attempt was made to find average sedimentation rates for the decades just before and after the emplacement of the Hwy. 1 bridge, this was not entirely possible due to the very high uncertainty (reported throughout at the 2σ level) around all dates in the first half of the twentieth century. For example, to ensure that the uncertainties did not overlap, in SC-11 the shortest interval that could be used to calculate a pre-bridge sedimentation rate was between 1850 CE ± 50 yrs and 1931 CE ± 30 yrs. Additionally, no post-bridge emplacement sedimentation rate could be calculated without including the 1955 levee breach in order to avoid age inversion. This flood event contributed to high sedimentation rates that likely overshadow sedimentation rate changes over intervening decades between bridge emplacement and the crevasse-splay deposit.

Results

Stratigraphic Description and Physical Characterization

Sediment Cores

Stratigraphic descriptions for all cores can be seen in Figs. 2-5. Core SC-6 ranges from medium silt to gravelly fine sand (D_{50} of 12-179.2 µm) (Fig. 2). Multiple coarse strata were found, including very fine sand (D_{50} = 130 µm, D_{90} = 320 µm) from 118-131 cm, gravelly fine sand (D_{50} = 152 µm, D_{90} = 7117.5 µm) between 145 and 152 cm, gravelly fine sand (D_{50} = 149 µm, D_{90} = 2901.3 µm) between 156 and 165 cm, and fine sand (D_{50} = 166.1 µm, D_{90} = 360.4 µm) from 235-265 cm. Core SC-11, situated closer to the current channel than SC-6, is predominantly composed of medium to very coarse silts similar to the marsh platform cores SC-6, interspersed with a few coarser sand and gravelly horizons (Fig. 3). There is a very fine sand interval from 159 to 171 cm (D_{50} = 124.4 µm, D_{90} = 244 µm), a gravelly fine sand interval (D_{50} = 120 µm, D_{90} = 2518 µm) between 200 and 211 cm and very coarse sand (D_{50} = 1170 µm, D_{90} = 8076 µm) from 257 cm to the base of the core.

As previously mentioned, core SC-9 was collected from an abandoned channel that had been occupied until its relocation associated with the bridge emplacement in 1938 CE. It contains two coarse deposits dominated by gravelly coarse sand (average D_{50} = 849.3 µm, D_{90} = 9162 µm) extending from depths of 66-109 cm, with a diffuse lens of gravelly fine sand (D_{50} = 139.4 µm, D_{90} = 7805.2 µm) from 90-95cm (Fig. 4). These are situated between two units of medium to coarse silt, with the upper unit (0-66 cm) characterized by

abundant organic material. Core SC-10 was located in the same channel as SC-9 and also contained organic rich medium to very coarse silts from 0-66 cm depth (Fig. 5). The core bottomed-out in gravelly medium to coarse sands (average D_{50} = 616.5 µm, D_{90} = 14038 µm) starting at 66 cm and extending to the base of the core at 88 cm. Additional particle size parameters can be seen in Figs. 10-13.

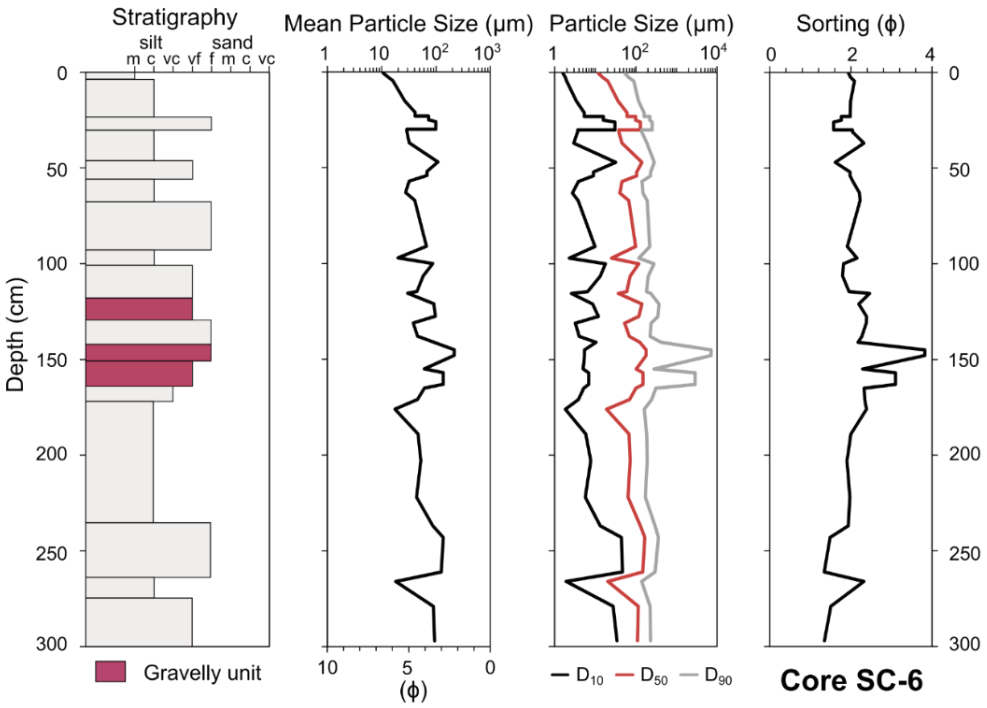

Fig. 3. Sediment characteristics for core SC-6.

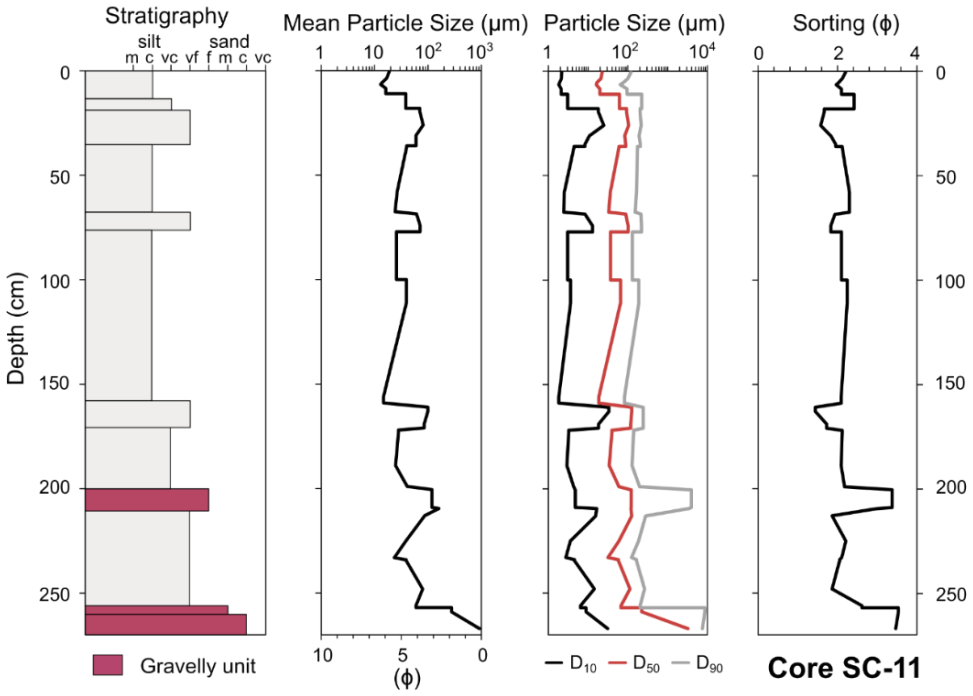

Fig. 4. Sediment characteristics for SC-11.

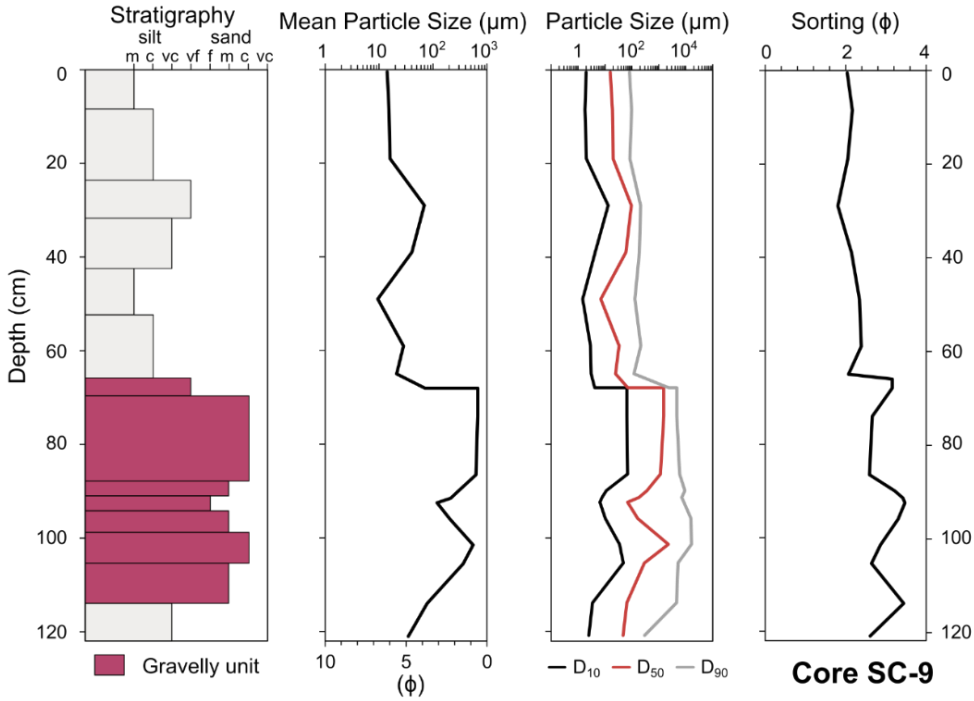

Fig. 5. Sediment characteristics for core SC-9.

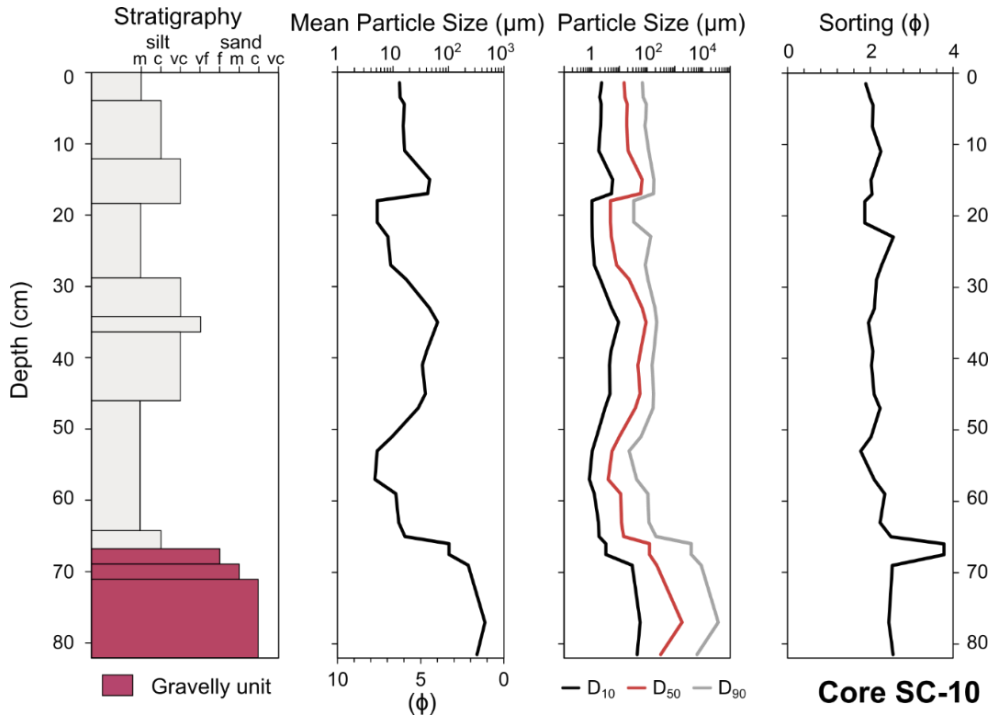

Fig. 6. Sediment characteristics for core SC-10.

Surface Sediment Samples

The particle size distribution of sediment collected from the Scott Creek beach varied depending on transect location, and geomorphic position within the transect (see Fig. 6 and Table 2). Samples collected from the nearshore (NS) were bimodal with a medium to coarse sand peak and a very coarse sand peak. FS1 samples had symmetrical, unimodal particle size distributions with identical modes at 429.7 μm. FS2 samples, collected ~10 m farther up the beach profile than FS1, were slightly coarser (mode at 471.7 μm) but still symmetrical and unimodal. Samples collected from the beach berms (B) had three distinct modes at 471.7 μm, 1741 μm, and 1316 μm. Samples collected from behind the berm (BB) had more variability across the three transect, but each shared a mode at

517.8 µm. The T1_BB sample was the coarsest with other modes at 3680 µm and 6005 µm. Additionally, ASC samples were bimodal to trimodal with a medium to coarse sand peak paired with a very coarse sand peak and/or a very fine gravel peak (T2_ASC).

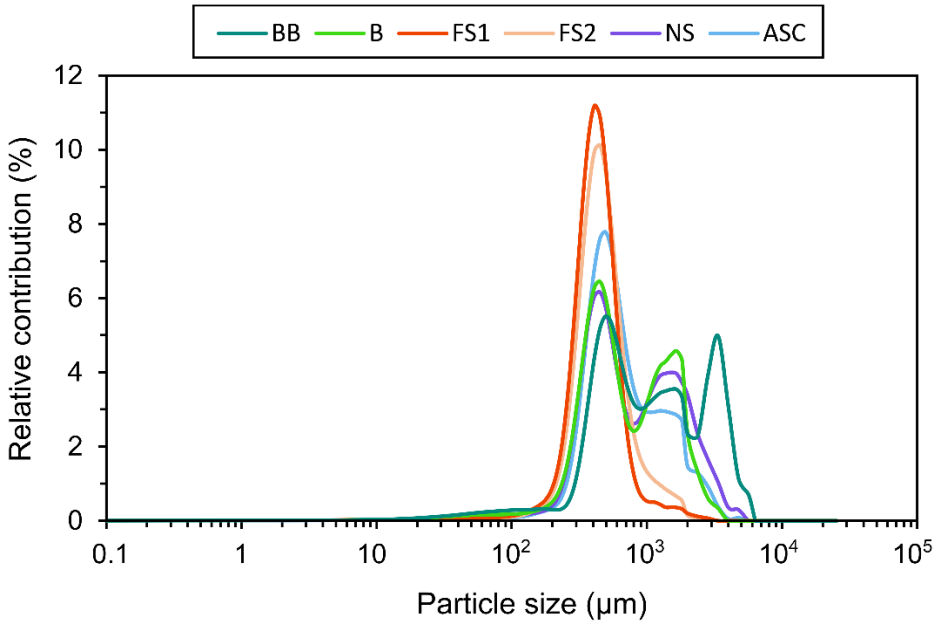

Fig. 7. Particle size distribution for surface sediments from different beach environments (averaged across the three transects). Abbreviations refer to the following: back berm (BB), top of berm (B), foreshore 1 (FS1), foreshore 2 (FS2) - collected ~10 m landward from FS1, nearshore (NS), flooded beach channel (ASC).

Table 2. Sediment characteristics for surface sediment samples collected from Scott Creek Beach

Transect	Location	Mean (μm)	Mean (φ)	Modes (μm)	Modes (φ)
T1	Nearshore	780.7	0.357	471.7, 1741	1.09, -0.798
T2	Nearshore	494.5	1.02	429.7, 1199	1.22, -0.260
T3	Nearshore	893.0	0.163	1444.5, 517.8	-0.529, 0.951
T1	Foreshore 1	412.0	1.28	429.7	1.22
T2	Foreshore 1	413.4	1.28	429.7	1.22
T3	Foreshore 1	410.0	1.29	429.7	1.22
T1	Foreshore 2	464.5	1.11	471.7	1.09
T2	Foreshore 2	451.4	1.15	471.7	1.09
T3	Foreshore 2	456.8	1.13	471.7	1.09
T1	Berm	476.8	1.07	471.7, 1741, 1316	1.09, -0.798, -0.395
T2	Berm	893.6	0.162	1741, 471.7	-0.798, 1.09
T3	Berm	638.5	0.647	471.7, 1741, 1316	1.09, -0.798, -0.395
T1	Back berm	1038.6	-0.055	3680, 517.8, 6005	-1.87, 0.951, -2.58
T2	Back berm	780.7	0.357	517.8, 1741, 3095	0.951, -0.798, -1.625
T3	Back berm	749.0	0.417	517.8, 1586	0.951, -0.664
T1	Channel	826.2	0.275	568.4, 1316	0.817, -0.395
T2	Channel	1209.9	-0.275	3095, 471.7, 1586	-1.63, 1.086, -0.664
T3	Channel	615.5	0.700	471.7, 1316	1.086, -0.395

The results of particle size analysis on channel samples can be seen in Fig. 7 and Table 3. In general, mean particle size increases upstream. The sand gravel transition can be seen between transects 2 and 3, as T3_TH has a gravel mode. Though mean particle size does not reach gravel until transect 4. The first two transects are unimodal fine sands with peaks at 203.7, 169, and 223.7 μm. Starting at transect 4, the samples become trimodal with significant gravel peaks and fine sand peaks. Samples collected from the marshy finger channel are coarse silt to very fine sand with peaks at 26.17 μm, 169 μm, and 116.4 μm.

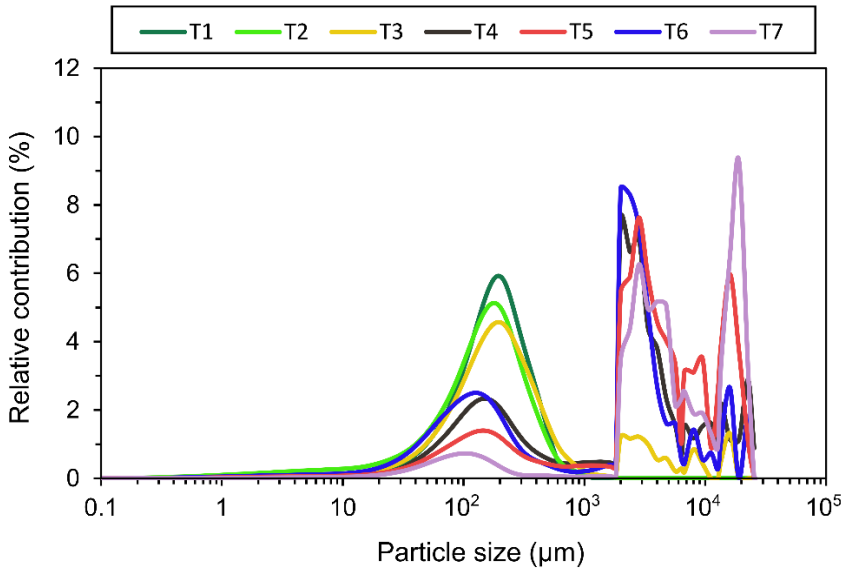

Fig. 8. Particle size distribution for surface sediments from seven channel transects (averaged across each transect). T1 is the farthest transect downstream.

Table 3. Sediment characteristics for surface sediment samples collected from Scott Creek

Transect	Location	Mean (µm)	Mean (φ)	Modes (µm)	Modes (φ)
T1	North	149.2	2.744	203.7	2.297
T1	South	142.8	2.808	203.7	2.297
T1	Thalweg	175.8	2.508	223.7	2.162
T2	North	122	3.036	169	2.566
T2	South	76.09	3.716	169	2.566
T2	Thalweg	178.2	2.488	223.7	2.162
T3	Thalweg	409.8	1.287	169, 3095, 2190	2.566, -1.625, -1.125
T3	Middle	142.2	2.814	203.7	2.297
T3	South	179.9	2.475	223.7	2.162
T4	North	391.4	1.353	169, 2190, 11950	2.566, -1.125, -3.576
T4	Thalweg	2022.4	-1.281	3095, 6005, 10355	-1.625, -2.584, -3.367
T4	Middle	570.1	0.811	2190, 3095, 127.8	-1.125, -1.625, 2.97
T5	North	2032.7	-1.023	13100, 6005, 3095	-3.711, -2.584, -1.625
T5	Middle	711.6	0.491	3095, 2190, 127.8	-1.625, -1.125, 2.97
T5	Thalweg	3376.2	-1.755	13100, 10355, 5210	-3.711, -3.367, -2.376
T6	Average	538.9	0.892	2190, 127.8, 17500	-1.125, 2.97, -4.124
T7	Average	611.9	-1.350	20800, 6540, 3095	-4.373, -2.709, -1.625
Finger	South	104	3.265	169	2.566
Finger	Middle	23.02	5.441	26.17, 116.4	5.258, 3.104
Finger	North	69.04	3.856	169	2.566

Radionuclide Results and Chronological Models

The deepest core, SC-6, generated the most robust chronological model, which consists of a combination of Pb-210ex, Cs-137, and radiocarbon dates (Table 4, Table 7). As expected, the highest Pb-210ex activities were found at the surface (Fig. 8A). The activity profile began with a surface value of 65.8 ± 18.3 Bq kg^{-1}, decreased to 27 ± 13.7 Bq kg^{-1} at 5cm depth, then quickly increase back to 58.7 ± 14.3 Bq kg^{-1} at 8 cm. Pb-210ex decreased down to zero at a depth of 15 cm, but a small peak in activity (14.7 ± 13.9 Bq kg^{-1}) was found between 20 - 23 cm. Radiocesium appeared at the surface and increases until peak activity (19.60 ± 1.90 Bq kg^{-1}) at 6.5cm. Below this, Cs-137 activity is quite low, aside from a minor peak (5.3 ± 1.2 Bq kg^{-1}) at 21cm.

Table 4. Dates used for the SC-6 age model

Depth (cm)	Age (year)	Dating method
0	2018	Date of collection
0.5	2015 ± 5	Pb^{210}
1.5	2013 ± 5.5	Pb^{210}
2.5	2010 ± 6	Pb^{210}
3.5	2007 ± 6.5	Pb^{210}
4.5	2004 ± 7	Pb^{210}
5.5	2000 ± 7.8	Pb^{210}
6.5	1963 ± 3	Cs^{137}
10	1955 ± 3	Stratigraphy
22.5	1943 ± 31	Pb^{210}
24	1957 ± 3	Radiocarbon
28	1923 ± 45	Pb^{210}
41	1909 ± 56	Pb^{210}
65	1962 ± 1	Radiocarbon
156.5	1470 ± 16.5	Radiocarbon
285	696 ± 27	Radiocarbon

The age model for SC-9 was created using a combination of Cs-137 dates, stratigraphic evidence, and radiocarbon dates (Table 5, Table 7). Fallout radionuclide analysis revealed the onset of Cs-137 activity at 19 cm, with a prominent Cs-137 peak (38.85 ± 2.97 Bq kg^{-1}) at 13 cm depth (Fig. 8B). As previously mentioned, historical imagery from the early 20th century revealed that both SC-9 and SC-10 were collected from the main channel reach prior to the emplacement of the Hwy. 1 bridge. This suggests that the coarse deposits in both cores are channel sediments, and it can be inferred that the transition from coarse gravel to organic rich mud at 66cm occurred around 1938, when the channel was leveed and diverted under the bridge.

Table 5. Dates used for the SC-9 age model

Depth (cm)	Age (year)	Dating method
0	2018	Date of collection
13	1976 ± 2	Radiocarbon
13	1963 ± 3	Cs^{137} peak
19	1954 ± 3	Cs^{137} onset
66	1938 ± 3	Stratigraphy

The chronological model for SC-11 was created using combination of Pb-210ex, Cs-137, and radiocarbon dates, as well as stratigraphic evidence (Table 6-7). Pb-210ex activity in core SC-11 is similar to that of core SC-6 (Fig. 8C). Surficial activity was 58.7 ± 15.3 Bq kg^{-1}, but increased to 75.4 ± 19.0 Bq kg^{-1} at 7cm depth, and then decreased to 11.1 ± 10.7 Bq kg^{-1} around 18 cm. Excess Pb-210 then decreased to zero until the 40 cm interval, where activity spikes to 30.0 ± 17.8 Bq kg^{-1}, before decreasing again. Cs-137 activity was found at the surface (9.42 ± 1.79 Bq kg^{-1}), increasing slightly in the top 7cm,

and then decreased until 12 cm, below which it increased again and reached an overall peak of 34.8 ± 2.50 Bq kg^{-1} at 17 cm.

Table 6. Dates used for the SC-11 age model

Depth (cm)	Age (year)	Dating method
0	2018	Date of collection
0.5	2017 ± 4	Pb^{210}
1.5	2016 ± 4	Pb^{210}
2.5	2015 ± 4	Pb^{210}
3.5	2013 ± 5	Pb^{210}
4.5	2010 ± 5	Pb^{210}
5.5	2009 ± 5	Pb^{210}
6.5	2007 ± 6	Pb^{210}
7.5	2005 ± 6	Pb^{210}
8.5	2002 ± 6	Pb^{210}
9.5	2000 ± 7	Pb^{210}
10.5	1998 ± 7	Pb^{210}
11.5	1997 ± 7	Pb^{210}
13	1993 ± 8	Pb^{210}
17	1963 ± 3	Cs^{137}
20	1955 ± 3	Stratigraphy
52	1939 ± 30	Pb^{210}
54	1893 ± 65	Pb^{210}
56	1877 ± 80	Pb^{210}
58	1825 ± 128	Pb^{210}
77.5	1962 ± 1	Radiocarbon

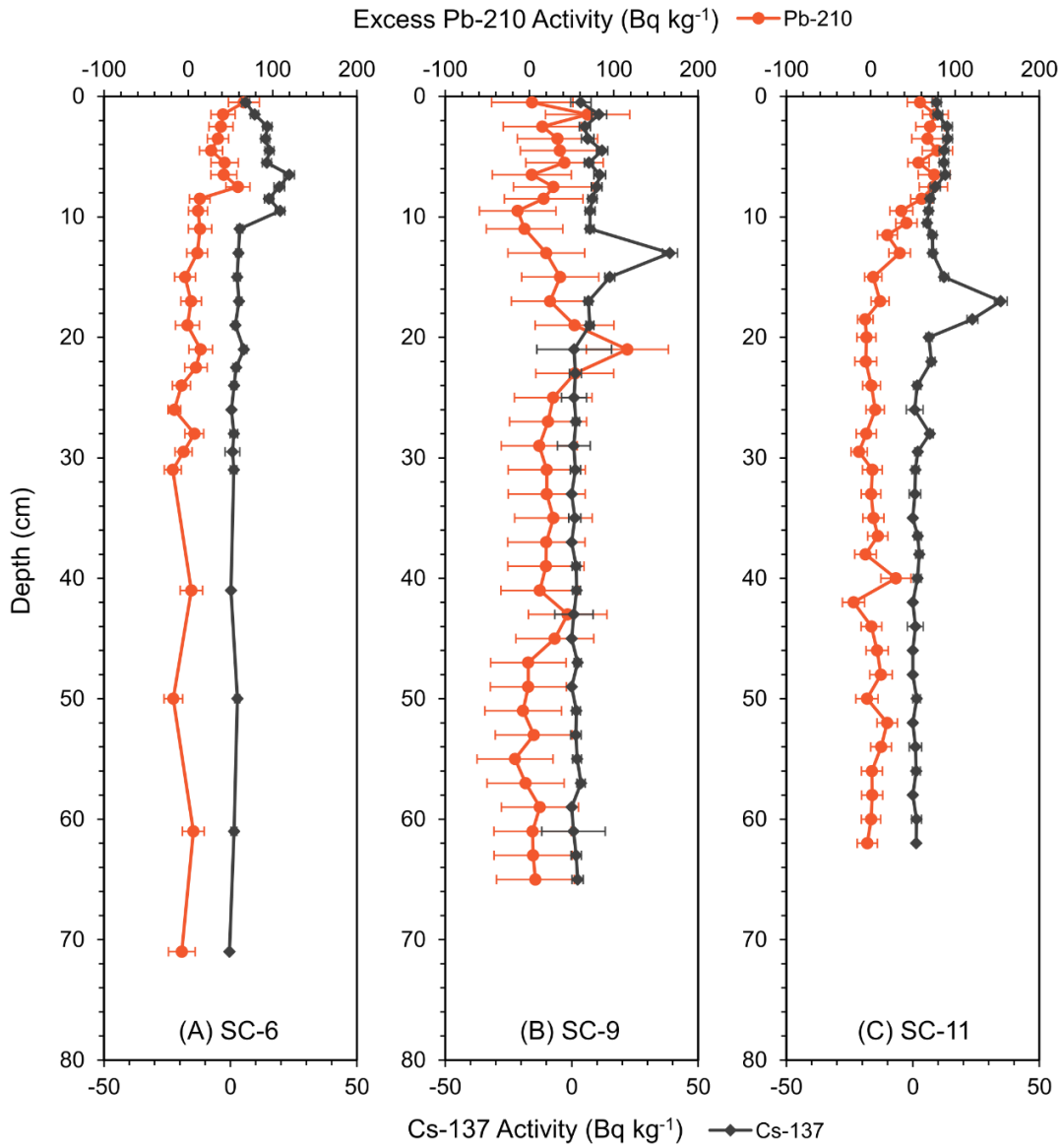

Fig. 9. Fallout radionuclide activity for cores SC-6, SC-9, and SC-11. Error bars are 1 sigma.

Table 7. Radiocarbon data

			UCI AMS Results					Calibration Results	
Core ID	Mean depth (cm)	Material type	Sample ID	Fraction modern ($F^{14}C$)	±	^{14}C age (BP)	±	2-Sigma range	Age (AD)
SC-6	24	Roots	209853	1.0583	0.0018	Modern		1956.8 – 1957.4	1957.1
SC-6	65	Roots	209854	1.3567	0.0021	Modern		1962.4 – 1962.7	1962.5
SC-6	156.5	Roots	209852	0.9529	0.0016	385	15	1449 - 1511	1469.5
SC-6	285	Roots	209851	0.8516	0.0045	1290	45	652 - 778	696
SC-9	13	Seeds	209855	1.3459	0.0023	Modern		1976.2 – 1977.7	1976.9
SC-9	55	Seeds	209856	0.9246	0.0015	630	15	1347 - 1392	1372
SC-9	116	Seeds	209857	0.8440	0.0014	1360	15	648 – 672	659.5
SC-9	122	Seeds	209858	0.9484	0.0028	425	25	1429 - 1491	1452
SC-10	87	Roots	209859	1.0531	0.0020	Modern		2007.7 – 2009.6	2008.8
SC-11	77.5	Roots	209860	1.3958	0.0024	Modern		1962.6 – 1962.8	1962.7

Fallout radionuclide evidence of the 1955 crevasse-splay deposit was found from 10-22 cm depth in the SC-6 and 18-38 cm depth in SC-11, which corresponds to a distinct very fine sand stratigraphic horizon. In both cases Pb-210ex activity decreased significantly through the identified interval, with increased activities found above and below. This weakened signal is likely the result of a rapid influx of Pb-210ex poor sediment (i.e. the crevasse splay). In SC-11 the peak in Cs-137 abundance dated to 1963 can be seen just above the rapid sedimentation event, providing further evidence that these massive fine sand deposits found on the North Marsh platform originated from the 1955 levee breach.

Particle Size Distribution Analysis

Particle Size Distribution Groups

The particle size distributions for all core samples (119 samples total) can be divided into five general groups based on their overall shape and mean particle size (Fig. 9). The first particle size distribution curve will be called group 1. In general, samples in group 1 are not necessarily unimodal, but have a distinct silt mode (28 μm, 5.15 φ), a very coarse silt mode (54 μm, 4.22 φ), a very fine sand mode at 126 μm (2.98 φ), and a fine silt mode (more like a hump upon a tail) at 8 μm (7.0 φ) (Fig. 9A). While each sample does not have all four of these modes, at least one is present in each. Some are unimodal, but they are all poorly to very poorly sorted mud or sandy mud. Sediments belonging in group 1 are mostly mesokurtic and fine skewed. The composite mean particle size of group 1 samples is 15.5 μm, or 6.13 φ, with a D_{50} of 18.4 μm or 5.94 φ. Group 2 is almost entirely unimodal and fine to very fine skewed (Fig. 9B). There is a primary fine sand mode at 129

μm (2.95 φ), with a very fine sand minor mode at 64 μm, 3.97 φ. A fine silt mode around 8 μm is also visible in some samples. These sediments are mesokurtic as well, with a mean particle size of 37.9 μm, or 4.76 φ, and D_{50} of 56.1 μm or 4.22 φ. Group 3 is unimodal, leptokurtic with a fine sand mode at 149 μm (2.75 φ) (Fig. 9C). They are very fine skewed and their mean particle size is higher (81.9 μm, 3.65 φ, D50 of 111 μm or 3.20 φ). Sediments belonging in Group 4 are mostly polymodal with one fine sand mode around 154 μm (2.70 φ) and a few much coarser gravel modes at 3600 μm, or -1.8 φ, and 6500 μm, or -2.7 φ (Fig. 9D). They are very poorly sorted and much coarser than the other groups, with a mean particle size of 190 μm, 2.22 φ and D_{50} of 582 μm or 1.95 φ. Group 5 only includes a few samples that did not fit into any of the other four groups (Fig. 9E). They are polymodal and very poorly sorted, similar to group 4, but are much finer (mean particle size of 11.3 μm, 6.54 φ, D50 of 6.99 μm or 6.98 φ). The most prominent mode is 6 μm (7.37 φ) fine silt but most of the modes present in groups 1 and 2 are also present in these samples.

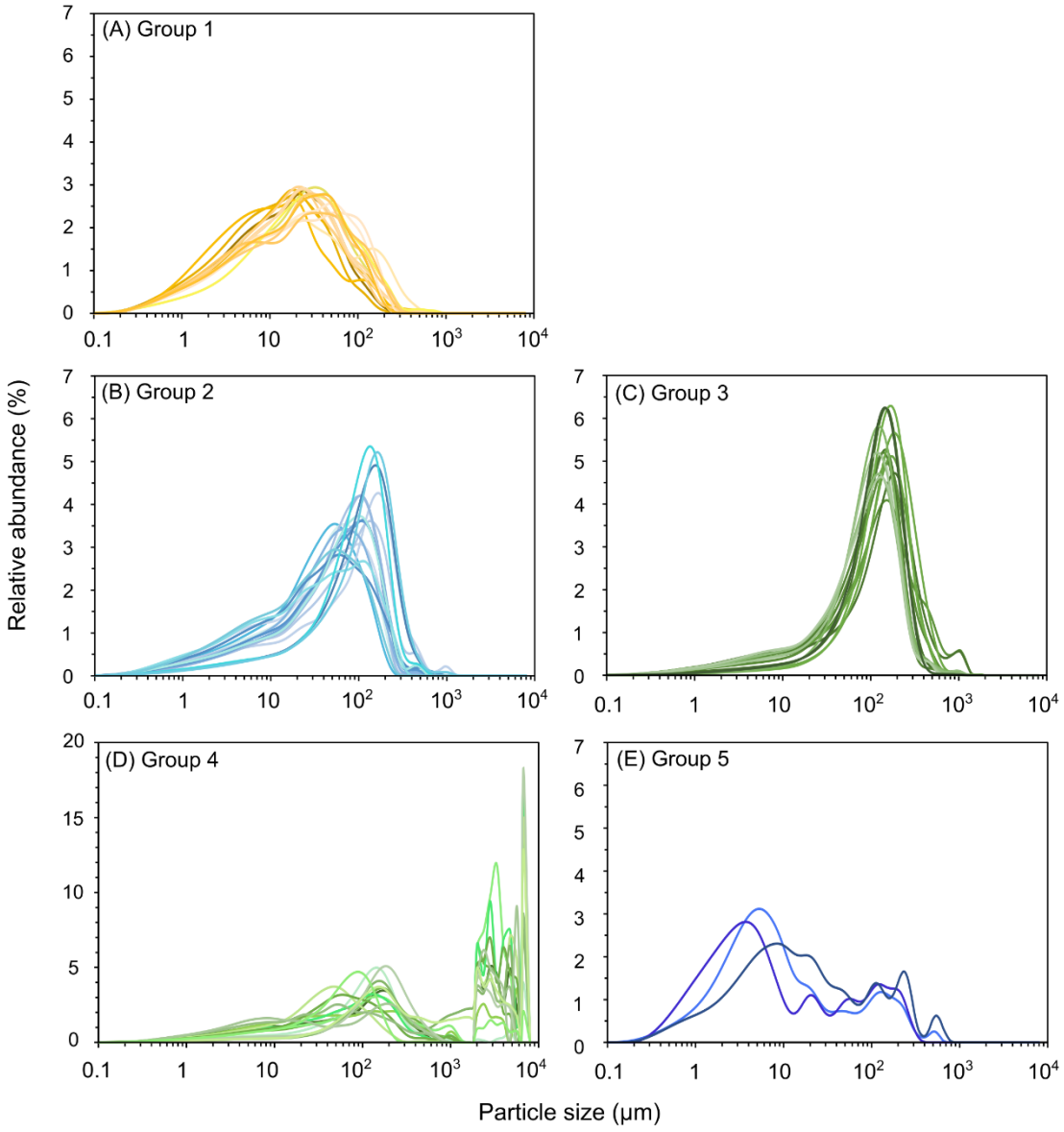

Fig. 10. Particle size distributions for the general particle size groups identified in the sediment cores.

Sediment from core SC-6 falls into group 1 from the present to 1956 CE (Fig. 10). The crevasse splay deposit between 10 cm and 22 cm belongs in group 2. The slightly coarser deposit below this can be categorized as group 3 and spans from 1938 to 1955 CE. Sediment deposited between 1900 and 1938 CE belongs in group 2. Between 1875 and

1900 CE is a thin band of group 3 that turns into group 2 until 1850 CE, or 59 cm depth. Around 68 cm or 1820 CE begins a coarse group 3 interval that extends down to 93 cm or 1725 CE. Below this are a few thin (3 to 10 cm) intervals of groups 1, 2, and 3, ultimately coarsening from group 1 down to group 3 just before 125 cm, or 1600 CE. At this depth, the first appearance of group 4 sediments occurs. This interval only lasts for 8cm then transitions to group 2 for 12 cm. There is a very thin interval of group 3 which transitions down to group 4 again at 144 cm or 1520 CE. Below this is a thin group 2 interval wedged between another group 4 package which extends down to 165 cm or 1415 CE. Thus, it appears that each package of group 4 sediments is buried by group 3 (or group 2) sediments that continue to fine upward or are replaced by another group 4 interval. The remainder of the core has thicker sediment packages (15 to 30 cm) similar to the top 95 cm, mainly alternative between groups 2 and 3 with two small group 1 intervals from 172 to 177 cm (1344 to 1375 CE) and 265 to 275 cm (740 to 785 CE).

Like SC-6, core SC-11 surface sediment particle size distributions belong in group 1 from the present to the mid-1990s (Fig. 11). Below this is a transition to group 2 sediments, which extend from 1996 to 1957 CE. The crevasses splay deposit from the 1955 flood event (18-38 cm) is composed of sediment belonging in group 3. Sediment are labeled as group 2 from 1955 down to 1100 CE with one coarser group 3 interval between 68 and 78 cm (1790 to 1840 CE). Much of the sediment variability seen in SC6 is not present in this core, especially between 1700 and 1100 CE. However, below 1100 CE, there are two coarse group 4 sediment packages with fining upward sequences similar to SC-6. Group 4 sediments extend from the base of the core up to 257 cm (132 to 353 BCE ± 500

years) and are covered by a 15 cm package of group 3 sediment. This fines upwards to group 2 at 237 cm and is topped with a fine 2 cm interval of group 3 sediment before the second group 4 package appears from 200 to 211 cm (470 to 568 CE ± 430 years). This package lies underneath a 30 cm interval of group 2 sediment, again suggesting a gradual fining upward pattern above each group 4 interval.

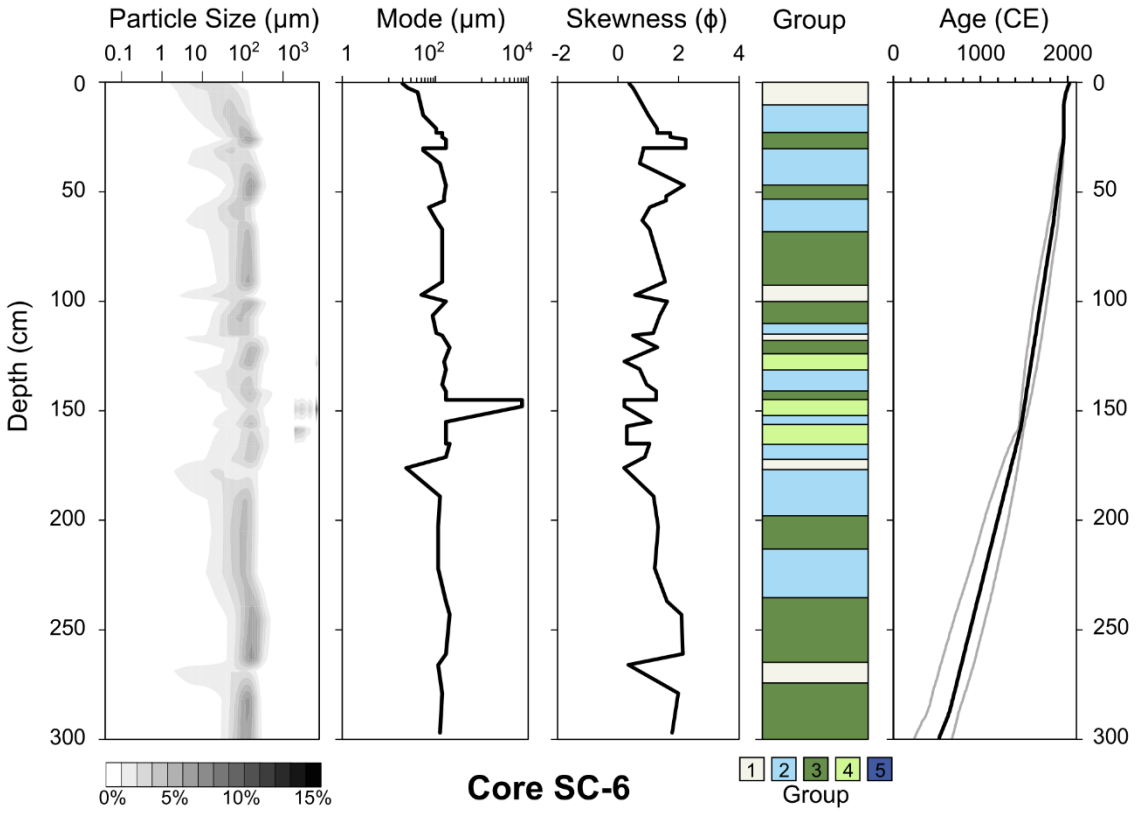

Fig. 11. Additional sediment characteristics for core SC-6, including downcore group designations and an age model.

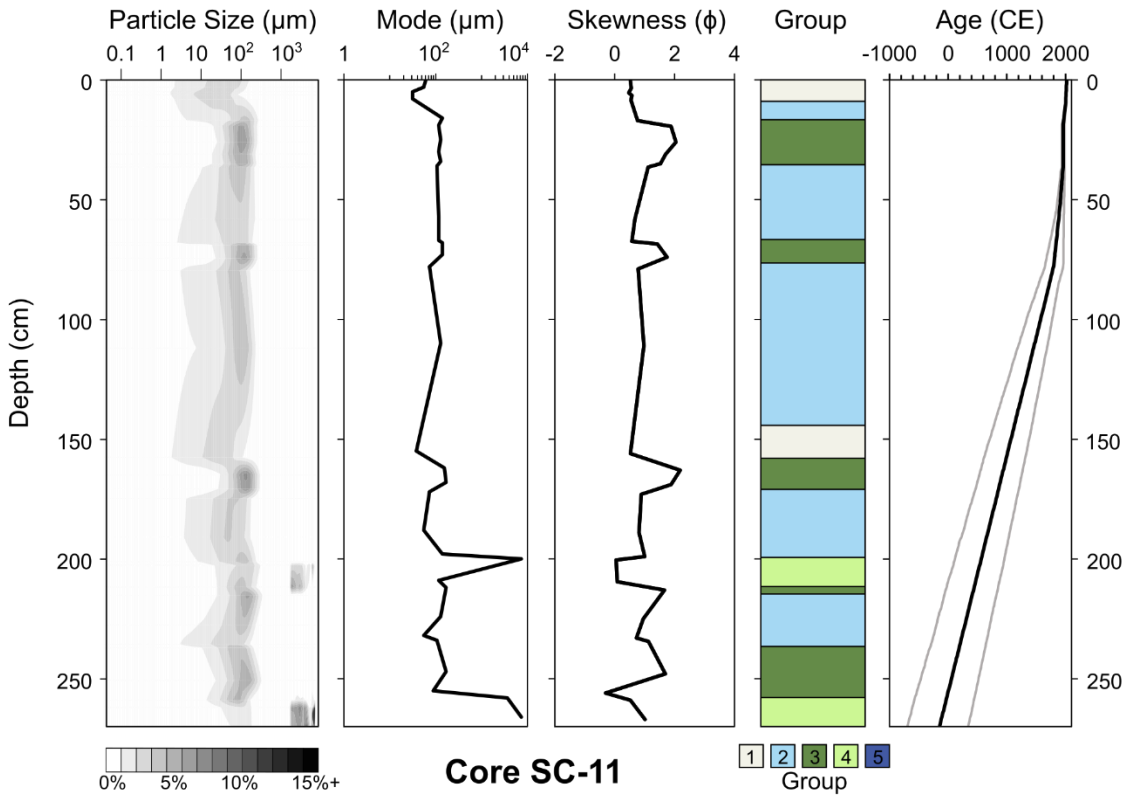

Fig. 12. Additional sediment characteristics for core SC-11, including downcore group designations and an age model.

Particle size distributions of sediments from the top 22 cm of SC-9 are characterized as group 1 (the present to 1955 CE) (Fig. 12). Between 1955 and 1949 CE, the sediment belongs in group 3, and shifts to group 2 until 1944 CE. There are group 5 sediments from 1944 to 1939 CE which coarsen downcore to become a group 1 interval during the time of levee building and channel relocation (1939 to 1932 CE). The sediment older than 1932 CE ± 10 yrs are group 4 until 1880 CE ± 27 yrs, ending on a short interval of group 1 sediment. In general, sediments are group 4 while the channel is located near SC-9 (pre-1930s), and fine upward until 1941 ± 10 yrs, when sediment begins to coarsen. The sediment continues to coarsen upcore, reaching group 3 in 1949 CE and persisting through the flood of 1955. Core SC-10 was not dated but it can be assumed that the beginning of

group 4 at 66 cm occurs in the 1930s like SC-9. This core also fines upward from the group 4 package, and alternates between group 1 and 2 (and a few cm of group 5) in the upper 50 cm (Fig. 13).

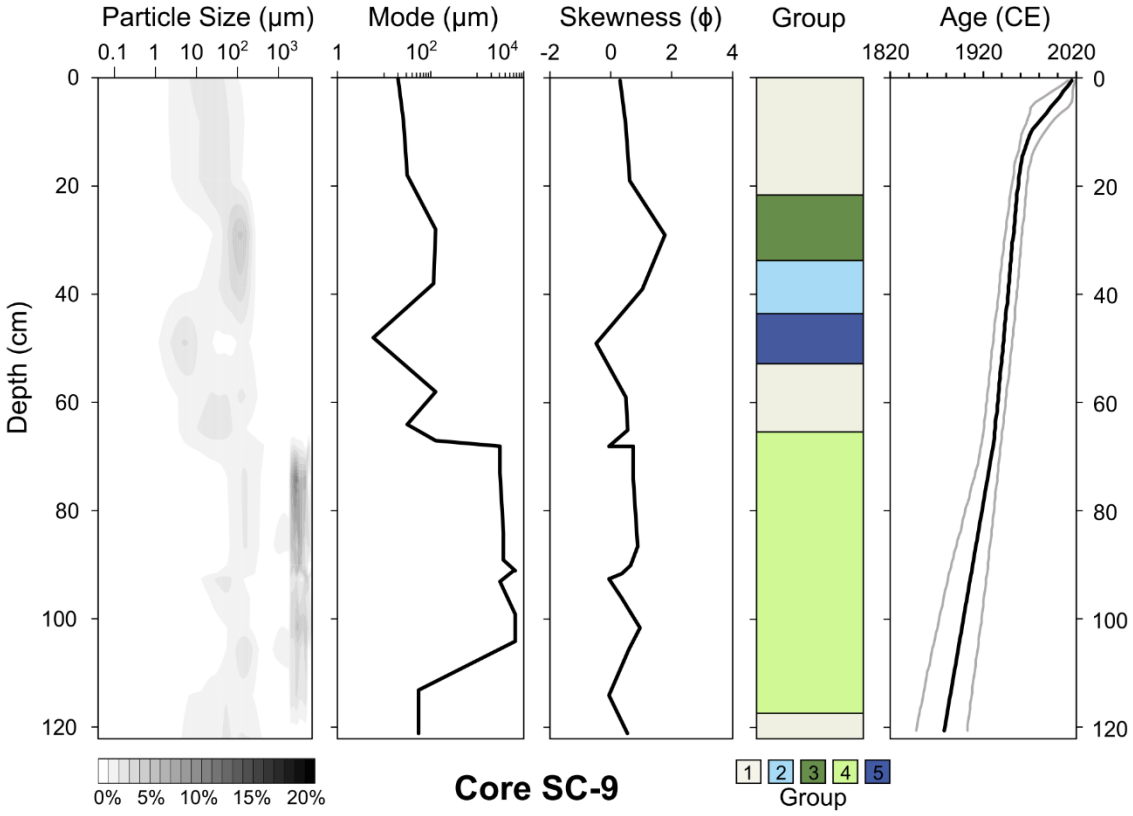

Fig. 13. Additional sediment characteristics for core SC-9, including downcore group designations and an age model.

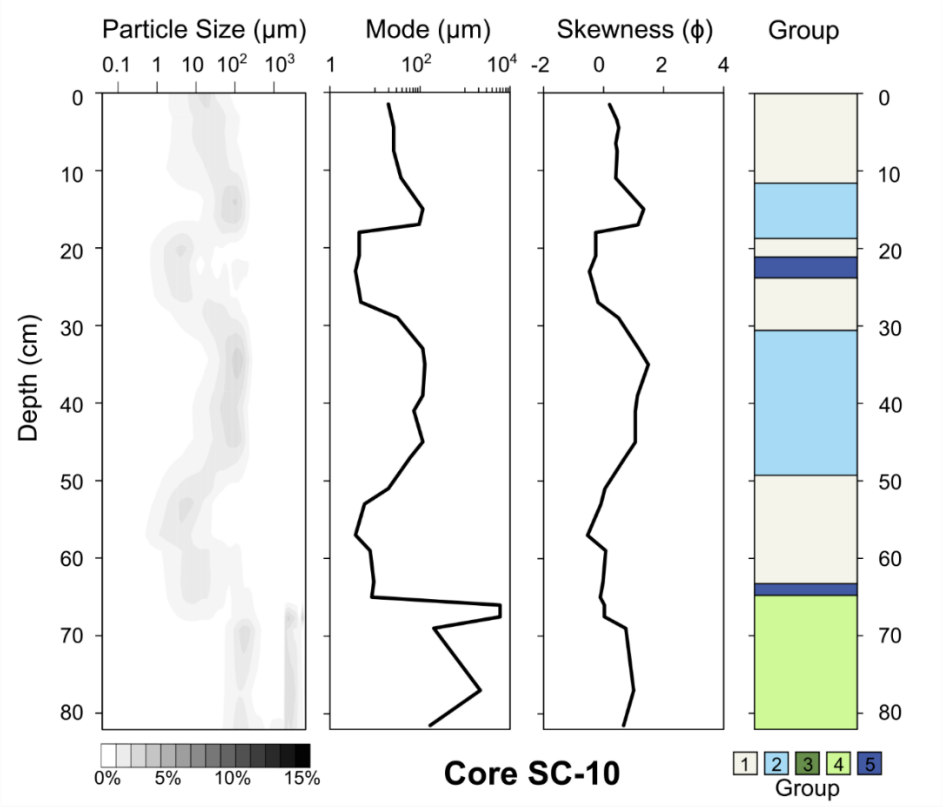

Fig. 14. Additional sediment characteristics for core SC-10, including downcore group designations. No age model was created for SC-10.

Bivariate Domains

To place these downcore group trends in geomorphic context, particle size statistics were plotted in bivariate space to distinguish between different depositional environments. The first plot, introduced by Tanner and modified by Lario, plots mean particle size (φ) versus sorting (φ) (Tanner, 1991; Lario *et al.*, 2002) (Fig. 14). This plot differentiates between channel and storm episodes, partially open to restricted estuary, and closed basin settling environment. Surface sediment samples from the beach and current channel were plotted, as were all core sediments in their corresponding particle size distribution groups. Groups 1 and 5 plot in the partially open to restricted estuary domain. Lower energy,

restricted estuary sediments plot in the bottom right region overlapping the closed basin settling environment domain. These sediments are probably deposited during periods of marsh flooding associated with barrier closure, as the estuary becomes a freshwater lagoon or somewhat restricted flooded estuary. Group 2 plots somewhat in the higher energy portion of the partially open to restricted estuary oval but mostly in the channel and storm episode domain, with mean values between 4 and 5.4 φ (average 4.77 φ) and sorting between 1.9 and 2.4 φ (average 2.15 φ). Group 2 sediments might also represent higher fluvial input to the estuary during larger storm events that result in flooding, as opposed to flooding strictly related to barrier closure. Group 3 plots in the lower portion of channel and storm episodes as well, with means between 2.8 and 4.2 φ (average 3.65 φ) and sorting between 1.3 and 2.2 φ (average 1.77 φ). Group 4 has higher (worse) sorting values and plots in the channel and storm episodes domain. These samples have more variability than the other three groups, with mean particle size ranging from 0.2 to 4 φ (average 2.22 φ) and sorting between 2.3 and 3.8 φ (average 3.06 φ). See Table 8 for defining characteristics and possible depositional environments associated with these groups.

Channel samples from T4 through T7 (and T3_TH) plot near group 4 or coarser, but in general have similar sorting values. Samples collected from the first three transects plot closer to group 3 as they have lower (better) sorting values and finer mean particle sizes. Beach samples plot in the bottom left of the channel and storm episode domain due to their very low sorting and mean particle size values. Mean values range between -0.05 and 1.3 φ (average 0.76 φ) and sorting between 1.0 and 2.0 φ (average 1.22 φ). All SCB_ASC samples plot in this same region as the rest of the beach samples.

Table 8. Particle size distribution group characteristics, associated end members, and the depositional environments they represent

PSD Group	Mean (μm)	Modes (μm)	End members	Depositional Environment
Group 1	15.5	Polymodal: 8, 28, 54, 126	EM-A, EM-B	Settling environment, restricted estuary/lagoon
Group 2	37.9	Unimodal: 64 or 126	EM-B	Partially open estuary, fluvial storm input
Group 3	81.9	Unimodal: 149	EM-D	Suspended load deposition, wave action/beach derived
Group 4	190	Polymodal: 154, 3600, 6500	EM-E, EM-D	Channel derived
Group 5	11.3	Polymodal: 6, 28, 64, 126	EM-A	Settling environment, restricted estuary/lagoon

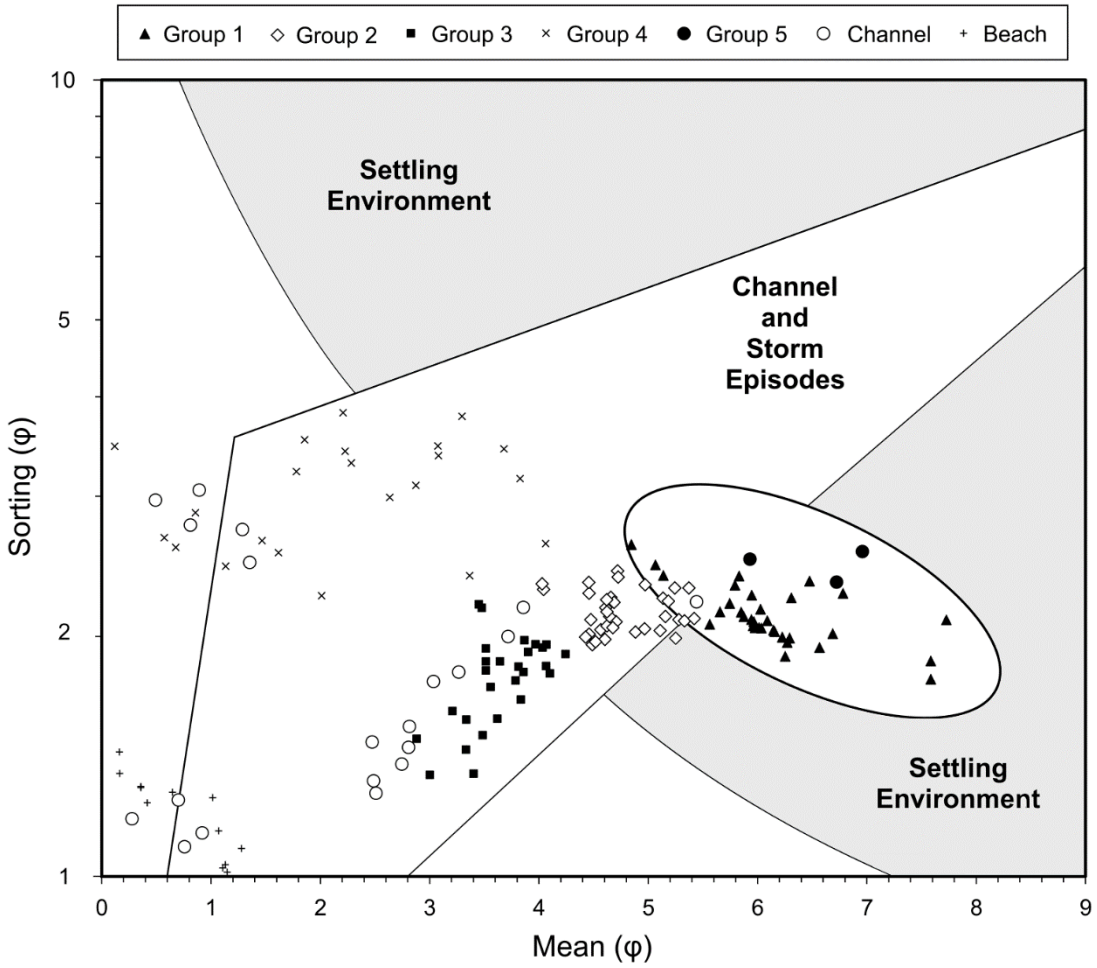

Fig. 15. Bivariate plot of mean particle size vs. standard deviation or sorting. Different depositional environment domains are from Tanner (1991) and Lario (2002).

The following additional bivariate plots were created: sorting vs skewness and kurtosis vs skewness (Figs. 15 and 16). These plots have been used in the literature to differentiate between beach and river sediments (Friedman, 1961; Moiola & Weiser, 1968). For these plots, a boundary can potentially be drawn between beach and river derived sediments to differentiate between the two different sources of sediment. In all three cases, the beach and channel samples from Scott Creek plot in two distinct regions, as expected. Channel samples that plot closest to the beach domain are from SCC_T1 and SCC_T2, the transects farthest downstream near the bridge and beach. In the sorting vs skewness plot, the beach samples are spread across a wide array of skewness values but in general plot markedly higher than the river and marsh samples. Beach samples in the kurtosis vs skewness plot also stand apart from the rest of the samples. All core samples from the marsh and abandoned channel plot in the river regions of the figures, with nothing plotting in the beach domain. Some samples from cores SC-6 and SC-11 plot in the transitional zone between the two. Specifically, SC-11 19-20 cm, 25-27 cm, 67-68 cm, 162-164 cm, and SC-6 25-27 cm, 242-244 cm, 260-262 cm, and 296-298 cm. All of these samples have particle size distributions that belong in group 3, but none of them are associated with the group 4 fining up sequences previously mentioned. In general, group 3 sediments plot closest to the beach samples in both plots, suggesting at least some beach sediments are brought upstream into the channel by wave overtopping. Group 1 and 5 sediments plot furthest away from the beach sediments, with group 2 plotting directly between 1 and 3.

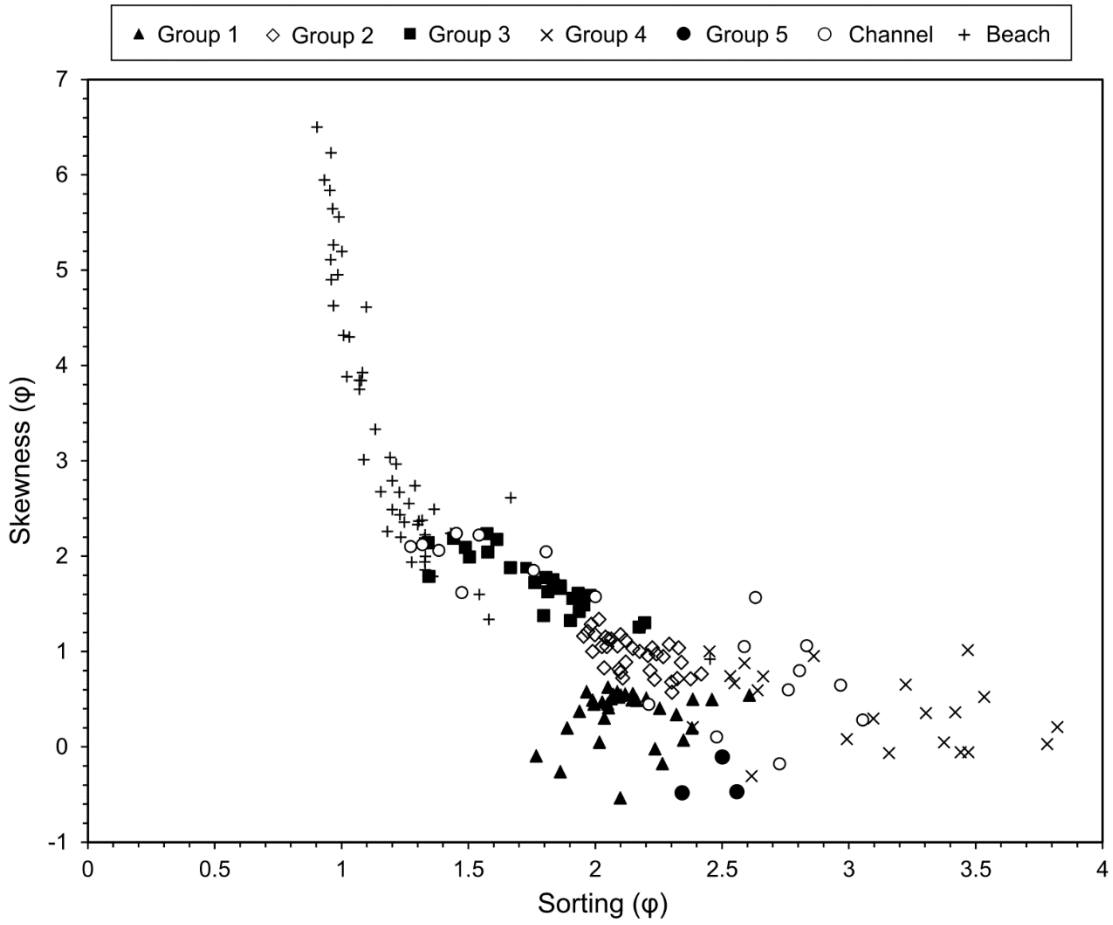

Fig. 16. Bivariate plot of sorting vs skewness. This plot differentiates between beach and river derived sediments.

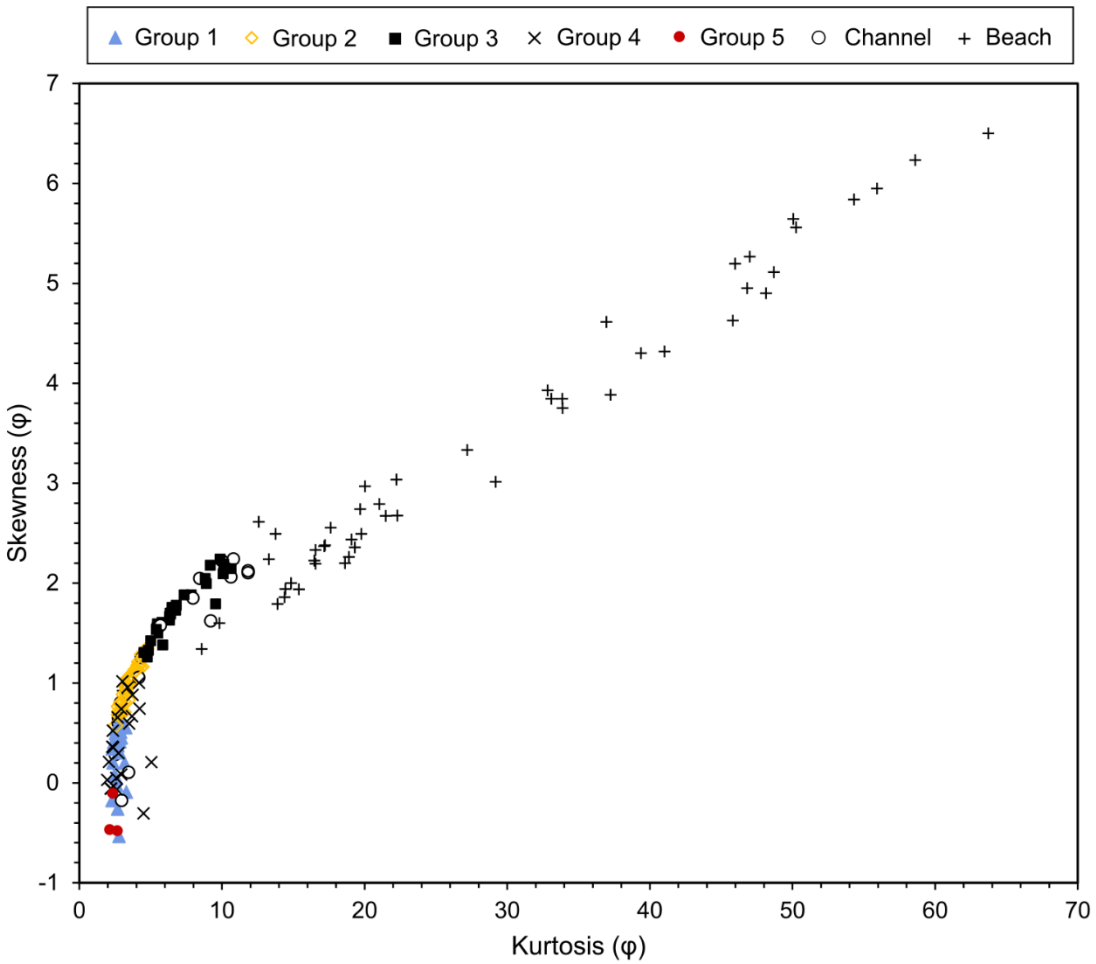

Fig. 17. Bivariate plot of kurtosis vs skewness. This plot also differentiates between beach and river derived sediments.

End Member Modelling

To further distinguish between the geomorphic environments these groups represent, five end members were derived from the EMMAgeo R package (Fig. 17). The five end members have a mean sample wise explained variance of 91% (with a minimum of 70%), so some combination of the five end members can reconstruct 91% of any sample's particle size distribution. The first end member (EM-A) explains 26% of the variance in the particle size distributions. It is a bimodal, very poorly sorted medium silt

with modes at 4.88 μm and 223.65 μm. This end member is mesokurtic and very coarse skewed (-0.582 φ). The second end member (EM-B) is a unimodal, very poorly sorted very coarse silt, and explains 26% of the variability in the particle size distributions. This end member is symmetrical (skewness of 0.195 φ) and leptokurtic with a mode at 66.5 μm. Next, EM-C is a trimodal, very poorly sorted very coarse silt explaining 10% of the sample variance. The modes are at 154 μm, 4.05 μm, and 1586 μm. This end member is very fine skewed (0.49 φ) and mesokurtic. The next end member (EM-D) is a unimodal, poorly sorted, very fine sand with a mode at 169 μm. This end member explains 28% of the sample variance and is very fine skewed (1.62 φ) and very leptokurtic. Finally, EM-E is trimodal and explains 9.9% of the sample variance. It has modes at 1199 μm, 295.9 μm, and 16.4 μm and is very poorly sorted. It is also very fine skewed (0.726 φ) and platykurtic.

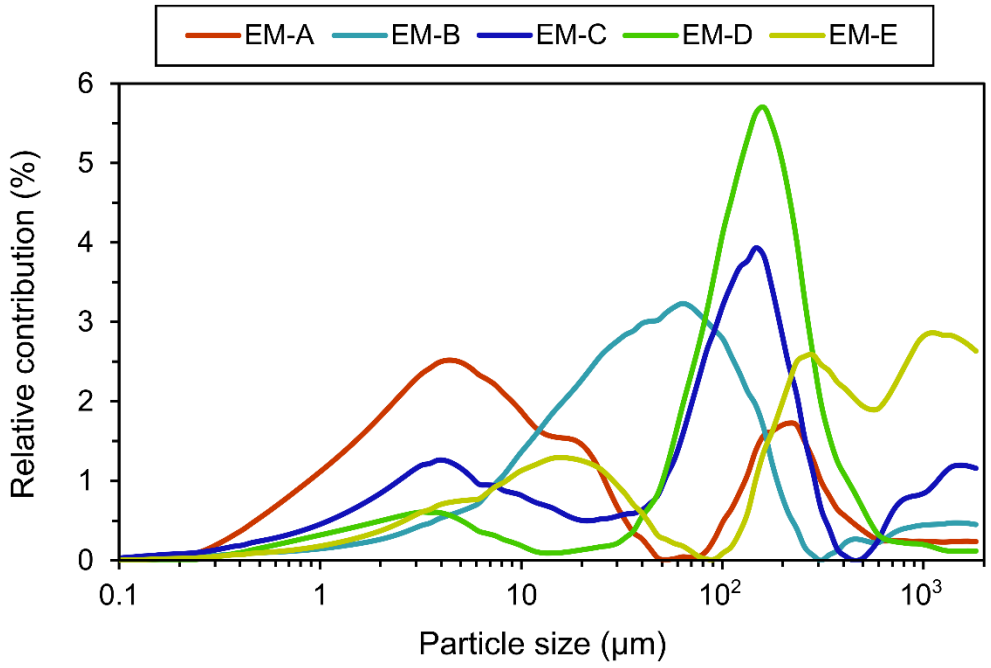

Fig. 18. Particle size distributions for the five end members derived from EMMAgeo.

Cores SC-6 and SC-11 are mostly composed of EM-B and EM-D (Fig. 18A and D). End member contributions appear to be at least somewhat related to the visually assigned particle size distribution groups. More specifically, intervals that are highly represented by EM-A are labeled as group 1 (SC-6 0-10 cm, 94-99 cm, 115 cm, 176 cm, 265-274 cm, and SC-11 0-10 cm, 145-158 cm). These intervals have high contributions from EM-A and EM-B. In some cases, EM-D contributes as well. Group 2 sediments are closely related to EM-B. Intervals labeled as group 2 are represented by EM-B with some contribution from EM-A, EM-C, and EM-D (SC6 10-22 cm, 30-46 cm, 54-68 cm, 110-115 cm, 132-140 cm, 168-172 cm, 177-198 cm, 212-234 cm, SC-11 10-19 cm, 35-67 cm, 78-145 cm, 171-199 cm, 215-235 cm). Group 3 appears related to EM-D as all intervals labeled group 3 have a significant contribution from EM-D in both cores. In the upper intervals (SC-6 22-30 cm, 47-53 cm, 69-92 cm, 100-109 cm, SC-11 18-38 cm, 68-77 cm, 158-172 cm) the samples are mostly represented by EM-D with variable contributions from EM-B and EM-C. In SC-6, the group 3 sediments associated with the group 4 intervals (group 3 - SC-6 116-122 cm, 140-144 cm) are mostly represented by EM-D with 20-30% EM-E as well. The rest of the group 3 samples in both cores are mostly EM-D with contributions from EM-B and EM-C. Group 4 intervals are mostly EM-D, with contributions from EM-A, EM-B, and EM-E (SC-6 122-131 cm, 145-151 cm, 155-165 cm, SC-11 200-208 cm, 260-269 cm).

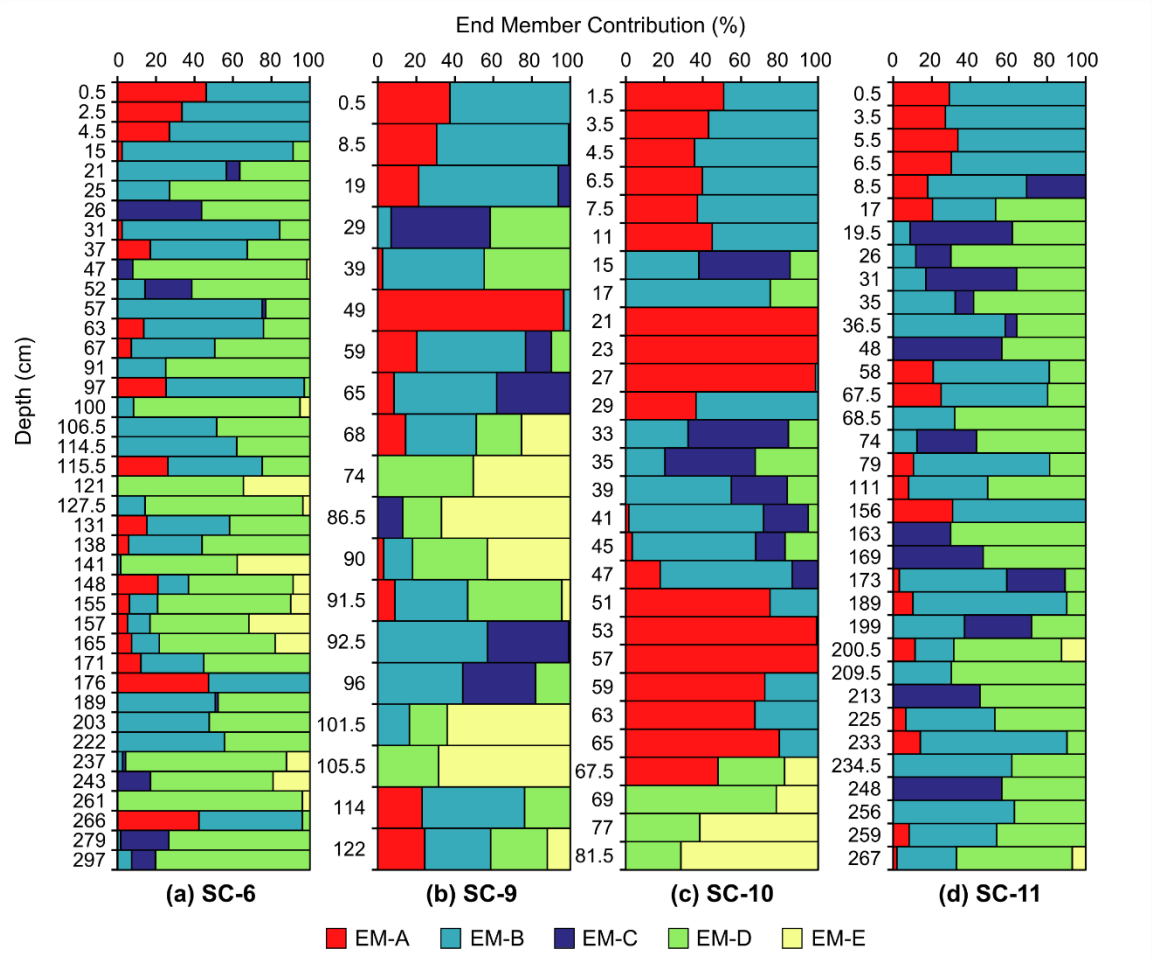

Fig. 19. Downcore end member contributions for cores SC-6, SC-9, SC-10, and SC-11.

The same general trends can be seen in the two abandoned channel cores (SC-9 and SC-10) (Fig. 18B and C). Intervals labeled group 1 are mostly represented by EM-A and EM-B with minor inputs from EM-D. Group 1 sediments from SC-10 have much high contributions from EM-A, especially between 50 and 65cm. In one instance, a package of group 1 sediment also has contributions from EM-E (SC-9 121-123 cm). Group 2 intervals (SC-9 35-44 cm, SC-10 12-18 cm, 32-49 cm) are a combination of EM-B, EM-C, and some contribution from EM-A or EM-D. The only group 3 interval (SC-9 23-34 cm) is mostly EM-C and EM-D, with contributions from EM-B. Group 5 samples (SC-9 45-53 cm, SC-

10 20-23 cm, 64-66 cm) can be explained with EM-A and very minor contributions from EM-B.

Group 4 sediments from SC-9 and SC-10 are more variable than those of SC-6 and SC-11. In SC-9, the top of the coarse package dating back to the 1930s (~66 cm) are 20% EM-A, 30% EM-B, 25% EM-D, and 25% EM-E. From 69 to 90 cm, the contributions from EM-A and EM-B disappear while contributions from EM-E increase (70% EM-E at 86.5 cm depth, or 1912). Contributions from EM-E disappear in the fine interval immediately below this, as contributions from EM-B and EM-C increase. This gradually transitions into the next coarse packet (45% EM-B, 35% EM-C, 20% EM-D at 96cm, shifting to 25% EM-D and 75% EM-E by 105.5 cm, or 1893). EM-A and EM-B reappear at the end of the package, which transitions back to group 1. As previously mentioned, this group 1 interval has contributions from EM-E, unlike all other group 1 sediments in any of the cores. The samples with high contributions from EM-D and EM-E (SC-9 69-89 cm, 97-113 cm) appear to be at the core of each of these coarse packages, with finer sediments with higher inputs from EM-A, EM-B, and EM-C bordering them. The same thing can be seen in SC-10. The group 4 sediment below 66cm can be split into two groups: intervals near the top (66-68 cm) with a high contribution from EM-A and some from EM-D and EM-E, and the rest (69-99 cm) which are only represented by EM-D and EM-E.

When the group 4 sediments from SC-9 and SC-10 are plotted in the Tanner bivariate space (Fig. 14), those with high contributions from the coarsest end member, EM-E, plot in a region separate from the rest. Samples between 69-89 cm and 97-113 cm in SC-9 and below 68cm in SC-10 plot in the channel domain near other coarse channel

samples from T4-T7. It is not surprising that these sediments resemble those of the current channel, as it was confirmed using aerial imagery that these sediments are from the channel prior to its relocation in the 1930s. The other channel samples with higher contributions from EM-A, EM-B, and EM-C plot in a separate, finer mean particle size region of the channel domain. These sediments (excluding the fine lens in SC-9) are from the top of the group 4 channel deposits and date back to the 1930s. They most likely represent the period of time in which the channel was being modified and ultimately abandoned by 1938. Based on these distinctions, group 4 can be split into two groups: group 4a for the sediments that plot near T4-T7 and represent active channel deposition, and group 4b for those that plot to the right of this region and represent more complicated channel dynamics.

When this boundary is applied to the group 4 sediments from SC-6 and SC-11, almost all samples plot in group 4b. Each of the group 4 sediment packages from SC-6 plot in the group 4b region and have relatively low contributions from EM-E. In SC-11, the group 4 interval from 200-212 cm and the top intervals of the group 4 package at the very base of the SC-11 (257 – 260 cm) also plot in group 4b. These group 4b sediments (and associated fining up sequences) must represent some form of channel deposition, though not necessarily in the active channel. The last sample (SC-11 267 cm), however, plots in group 4a, suggesting it is fundamentally different than the rest of the group 4 sediments in SC-6 and SC-11. It is most likely an active channel deposit, although it does not have a high contribution from EM-E like the other group 4a sediments in SC-9 and SC-10. This suggests that the bottom of core SC-11 captured the last remnants of an active Scott Creek

channel in the location of the current marsh platform, and that this approach can successfully identify periods of geomorphic change within this estuary.

Sedimentation and Sediment Accumulation Rates

Aside from providing valuable information regarding the stratigraphic signature of channel abandonment, the hydrologic modifications made during the 1930s vastly altered the connectivity between Scott Creek and its estuary. As previously mentioned, another aspect of this project was to investigate these changes in sedimentation on the marsh platform associated with the intense modifications to the channel. In SC-6 the sedimentation rate averaged 0.19 cm yr^{-1} between 354 CE and the present (Fig. 19 and Table 9). Sedimentation was low from 354 CE to 1880 CE (0.17 cm yr^{-1}) and then increased to 0.32 cm yr^{-1} between 1880 and 1937 CE. The average rate of sedimentation increased slightly to 0.38 cm yr^{-1} for the period spanning 1940 to the present. Within this time period sedimentation varied, with the highest rates found between 1954 and 1963 (1.8 cm yr^{-1}) driven by the 1955 flood event. After this period, sedimentation decreased to 0.23 cm yr^{-1} until 1976, continued decreasing to 0.11 cm yr^{-1} by 2009, and has since rebounded slightly to 0.16 cm yr^{-1}.

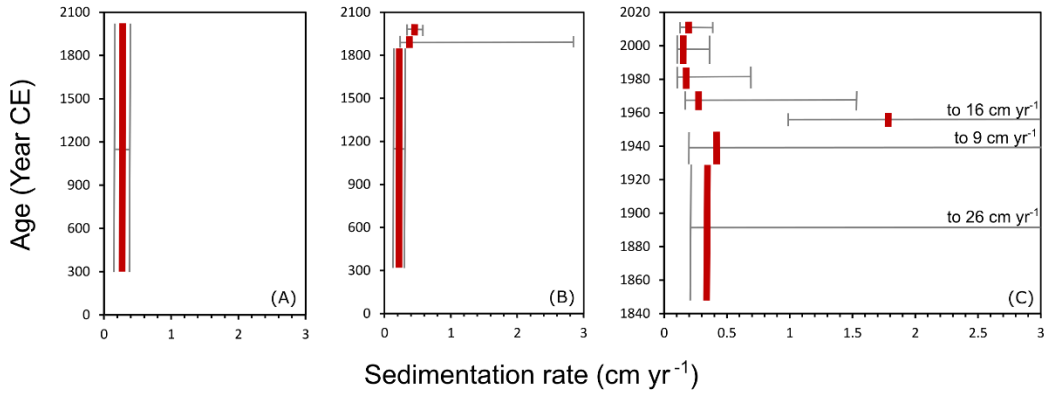

Fig. 20. Sedimentation rates for SC-6. (A). Average sedimentation rate for the entire timespan of the core (353 – 2018 CE). (B). Average sedimentation rates for three intervals: pre-1880, 1880 to 1937, and 1937 to the present. (c). Average sedimentation rates for smaller intervals over the last ~150 years.

Table 9. Sedimentation rates and sediment accumulation rates for SC-6

Depth Interval (cm)	Time interval (yr)	Sediment-ation rate (cm yr^{-1})	Sed. rate lowbound (cm yr^{-1})	Sed. rate upperbound (cm yr^{-1})	Accum ulation rate (g cm^{-2} yr^{-1})	Acc. rate lowbound (g cm^{-2} yr^{-1})	Acc. rate upperbound (g cm^{-2} yr^{-1})
0 - 317.5	354 - 2018	0.19	0.16	0.22	0.17	0.14	0.19
49.5-317.5	354 - 1880	0.17	0.14	0.21	0.17	0.14	0.20
31.5 - 51.5	1880 - 1937	0.32	0.16	2.86	0.26	0.13	2.34
0 - 30.5	1940 - 2018	0.38	0.30	0.52	0.27	0.22	0.37
33.5 - 59.5	1850 - 1931	0.32	0.18	26.0	0.26	0.14	21.1
24.5 - 33.5	1931 - 1954	0.39	0.16	9.00	0.35	0.14	8.05
24.5 - 8.5	1954 - 1963	1.78	0.94	16.0	1.30	0.69	11.74
5.5 - 8.5	1963 - 1976	0.23	0.13	1.50	0.14	0.08	0.92
3.5 - 5.5	1976 - 1991	0.13	0.07	0.67	0.07	0.04	0.37
1.5 - 3.5	1991 - 2009	0.11	0.07	0.33	0.06	0.04	0.17
0 - 1.5	2009 -2018	0.16	0.10	0.36	0.08	0.05	0.17

Sedimentation rates were also calculated for channel core SC-9 (Fig. 20 and Table 10). We found high sedimentation (1.00 cm yr^{-1}) from 1889 to 1918, then an increase to 1.36 cm yr^{-1} between 1918 and 1943. Sedimentation increased further to 1.76 cm yr^{-1} from 1943 to 1960, likely a result of the 1955 flood event. After 1960, sedimentation rates decreased to 0.35 cm yr^{-1} and fell even lower (0.2 cm yr^{-1}) between 1988 and the present. Higher sedimentation in this area in the early 1900s was due to its location within the main channel. Sedimentation remained high post-channel abandonment because of its low-lying position relative to the marsh platform during the 1955 flood event. However, sedimentation rates over the past 6 decades at SC-9 are comparable to those encountered elsewhere in the North Marsh.

Trends similar to SC-6 can be seen in SC-11, which averaged 0.14 cm yr^{-1} from 476 CE to the present (Fig. 21 and Table 11). Sedimentation rates averaged 0.10 cm yr^{-1} between 476 CE and 1731 CE, increased to 0.20 cm yr^{-1} until 1936, and then increased to 0.52 cm yr^{-1} between 1936 and the present. In the last century, higher sedimentation rates were detected between 1927 and 1987 (0.55 cm yr^{-1}), which decreased to 0.29 cm yr^{-1} until 2004, and rebounded back to 0.6 cm yr^{-1} in the last decade. Additionally, temporal patterns of sediment accumulation rates followed those of sedimentation rates for all three cores, suggesting these trends are not the result of dry bulk density differences (i.e. compaction at depth or abundant lower density organic rich material towards the surface) (Tables 9-11).

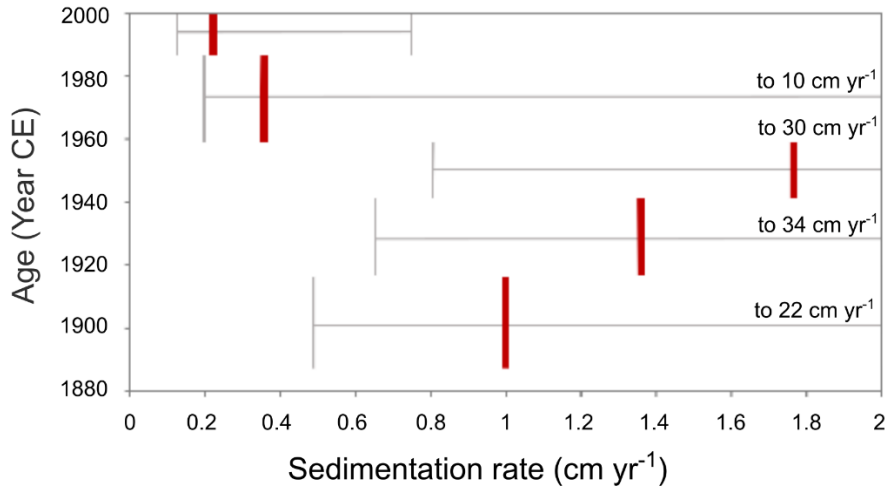

Fig. 21. Sedimentation rates for SC-9.

Table 10. Sedimentation rates and sediment accumulation rates for SC-9

Depth Interval (cm)	Time interval (yr)	Sedimentation rate (cm yr^{-1})	Sed. rate lowbound (cm yr^{-1})	Sed. rate upperbound (cm yr^{-1})	Accumulation rate (g cm^{-2} yr^{-1})	Acc. rate lowbound (g cm^{-2} yr^{-1})	Acc. rate upperbound (g cm^{-2} yr^{-1})
0 – 6.5	1988 - 2015	0.22	0.12	0.75	0.10	0.05	0.32
6.5 – 16.5	1960 - 1988	0.36	0.2	10.0	0.20	0.11	5.56
16.5 – 46.5	1943 - 1960	1.76	0.81	30.0	1.33	0.61	22.7
46.5 – 80.5	1918 - 1943	1.36	0.65	34.0	1.04	0.50	25.9
80.5 – 123	1889 - 1918	1.00	0.49	22.0	1.11	0.54	24.4

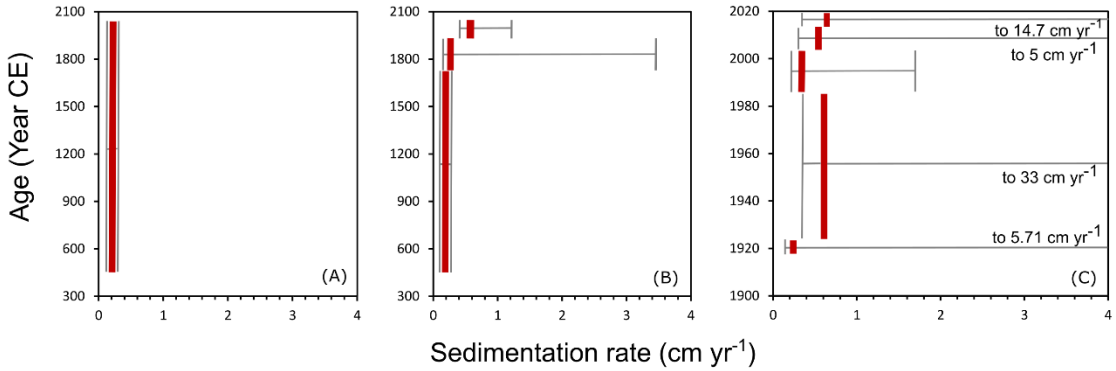

Fig. 22. Sedimentation rates for SC-11. (a). Average sedimentation rate for the timespan of the core (476 – 2018 AD). (b). Average sedimentation rates for three intervals: pre-1730, 1730 to 1936, and 1936 to the present. (c). Average sedimentation rates for smaller intervals over the last ~100 years.

Table 11. Sedimentation rates and sediment accumulation rates for SC-11

Depth Interval (cm)	Time interval (yr)	Sedimentation rate (cm yr^{-1})	Sed. rate lowbound (cm yr^{-1})	Sed. rate upperbound (cm yr^{-1})	Accumulation rate (g cm^{-2} yr^{-1})	Acc. rate lowbound (g cm^{-2} yr^{-1})	Acc. rate upperbound (g cm^{-2} yr^{-1})
0 - 208.5	476 - 2018	0.14	0.10	0.18	0.11	0.08	0.15
84.5 -208.5	476 - 1731	0.10	0.08	0.16	0.09	0.07	0.15
42.5 - 84.5	1731 - 1936	0.20	0.10	3.50	0.17	0.08	2.85
0 - 42.5	1936 - 2018	0.52	0.36	1.12	0.37	0.26	0.80
0 - 2.5	2014 - 2018	0.60	0.31	14.7	0.23	0.12	5.72
2.5 - 7.5	2004 - 2014	0.50	0.26	5.00	0.25	0.13	2.47
7.5 - 12.5	1987 - 2004	0.29	0.17	1.67	0.18	0.10	1.03
12.5 - 45.5	1927 - 1987	0.55	0.30	33.0	0.46	0.25	27.7
45.5 - 85.5	1721 - 1927	0.19	0.09	5.71	0.16	0.07	4.63

Discussion

Marsh History

Grouping sediment samples according to particle size distributions highlighted stratigraphic variation due to changes in depositional processes within Scott Creek estuary and channel over the last ~2,000 years. Plotting the sediment packages in defined bivariate domains (Tanner, 1991; Lario *et al.*, 2002) helped diagnose the depositional environments associated with different sediment groups, and end member modelling using EMMAgeo further captured the variability within the defined groups. Most noteworthy were the coarsest sediment packages in the two marsh platform cores (SC-6 122-131 cm, 145-151 cm, 155-165 cm, SC-11 200-208 cm, 260-269 cm). These coarse group 4 sediments resemble the channel deposits in the basal portions of SC-9 and SC-10 and plot in the channel depositional domain, suggesting that they are, in fact, channel deposits. This alone is strong evidence of a different channel configuration than the one prior to human intervention in the early twentieth century. However, further analysis suggests a more complicated story.

End member analysis indicated some variability within the channel deposits from SC-9 and SC-10. Channel sediments from the early 1930s (and in the SC-9 90-95 cm fine lens) display different end member distributions than the rest of the sediment in the channel deposits. Farmers began leveeing Scott Creek as early as 1930 (ESA, 2012) and the bridge was completed in 1938, but it is unclear exactly when the channel was relocated, and how quickly the process of converting a through-flow channel to a settling dominated

depositional feature was achieved. Sediments from this time period have very little to no contribution from EM-E, the characteristic channel end member, while the rest of the channel sediments are 20 – 80% EM-E. Also, while the sediments with high contribution from EM-E plot near current channel sediments in the Tanner bivariate diagram (group 4a), the others create a sub-region group 4b. This suggests that there are fundamental differences between the sediments deposited during active channel conditions and those from the channel while it was being diverted, and that perhaps this information could be used to refine interpretations of channel sediments found in the marsh platform cores.

Several fining up sequences were identified in the sediment cores from SC-6 and SC-11. Each group 4 channel deposit sits below a finer group 2 or 3 interval that continues to fine upward. In SC-6, there are three of these sequences stacked atop one another that are each no more than 20 cm thick. The group 2 and 3 sediments associated with these channel deposits cluster near one another in the Tanner bivariate diagram, and some of the group 3 sediments also have contributions from coarse EM-E, suggesting these finer sediments are genetically related to the channel sediments as opposed to separate unrelated depositional events. However, all of the channel sediments plot in group 4b in the Tanner bivariate diagram, which isn't considered the active channel domain. This indicates that these sediment packages are fluvially derived but were deposited somewhere outside of the active channel and should not be confused with active channel fill.

The fining up sequences from the group 4 sediment also occurs in SC-11, but there are key differences. Only two of these fining up sequences were found in SC-11 and they are much thicker (40-60cm) than those from SC-6. The channel sediment from SC-11 200-

210 cm and 257-265 cm plot in the group 4b region of the Tanner diagram, and the group 2 and 3 sediments associated with these sequences also plot in the same area as those in SC-6. However, the very base of the core (SC-11 266-268 cm) plots in group 4a next to the upper transects of the current channel, indicating that around 142 BCE ± 516 yrs an active channel flowed across the location of SC-11. This sample has a 20% contribution from EM-E, and intervals deposited in the centimeters just above this sample plot in group 4b and have no contribution from EM-E, suggesting that this particular sequence is a signature of channel abandonment.

Aside from human alteration, there are many mechanisms that result in channel abandonment, including meander bend cutoffs and channel avulsion (Fisk, 1947; Allen, 1965). Typically, there are multiple phases of channel abandonment, beginning with an initial shift of some of the stream's discharge to a new channel, although the degree to which water and sediment splits between the two bifurcates is highly dependent on several factors. These include the morphology of both the bifurcate zone and the nearest upstream channel meander, the downstream channel slope and roughness of both bifurcates, and the characteristics of the incoming sediments (Gray *et al.*, 2016). Sediment aggradation in the old channel is dictated by the amount of both sediment and water being split between the two bifurcates. Abandoned channels that receive very little sediment will obviously aggrade very slowly, while channels with higher connectivity may continue to receive bedload and suspended load that is deposited depending on the capacity of the diverted flow to transport it. As abandonment progresses, sediment deposition elevates or "plugs" the entrance and/or exit of the old channel, which further decreases hydro-sedimentological

connectivity and encourages even more discharge/sediment to divert to the new channel (Fisk, 1947; Hooke, 1995; Toonen *et al.*, 2012; Gray *et al.*, 2016). Because of this, each abandoned channel fill is unique. For example, some abandoned channels may have thick bedload deposits as a result of high sediment connectivity, while others only receive finer suspended load or pulses of sediment during high magnitude discharge events. However, most abandoned channels typically have preserved channel bed sediments that fine upward from very coarse sands to fine sand and silts (Bridge *et al.*, 1986; Toonen *et al.*, 2012).

It appears that the channel was located near SC-11 two millennia ago but began a process of abandonment. The fining up sequence that was deposited during channel abandonment is capped by another coarse deposit (SC-11 200-210 cm), which is most likely abandoned channel fill as pre-existing channel deposits typically have much larger particle size values than later fill deposits (Toonen *et al.*, 2012). This later coarse sediment could be the result of the channel being reoccupied during a large flood event (Lechner, 2009). In this situation, discharge from the newly rerouted channel temporarily reoccupies the abandoned channel and deposits its suspended load as stream velocity decreases. After 558 CE ± 422 yrs, there are no channel-like sediment deposit signatures in SC-11.

In 1415 CE ± 60yrs, the channel fining upward sequences appear in SC-6 and persist through ~1650 CE ± 70yrs. Some of the group 3 and 4 sediments have contributions from EM-E but nothing plots in the active channel domain. This, paired with the fact that these sequences are short lived, suggests that SC-6 was not at the location of an active channel but received several pulses of channel sediment. It is unclear where the main channel was, but it appears that after this period of channel activity, the area surrounding

SC-6 mostly received fluvially derived suspended sediments as a result of marsh flooding associated with storms and wave overtopping (group 2 and 3). Similarly, after channel abandonment and a brief reoccupation, sediments deposited in SC-11 were much finer and display significantly less variability (belonging in group 2 for the most part).

These group 2 sediments are most likely the result of fluvial input to the estuary (and the low-lying abandoned channel) during larger storm events that result in flooding, including during closed beach barrier lagoon phases with increased fluvial discharge from storm events (Cahoon *et al.*, 1996; Farnsworth & Milliman, 2003; Watson *et al.*, 2019). This type of deposition can account for most of the group 2 sediments in the upper 150 centimeters of SC-11, and in the upper 100 centimeters of SC-6. High energy wave events washing over the closed beach barrier may also play a smaller role in group 2 sediments. The unimodal group 3 sediments that plotted near the beach to river transition (not associated with channel sediments) in the Friedman plots may be from more energetic processes like wave action in open barrier conditions, which would carry coarser beach sands back into the estuary (Watson *et al.*, 2013). After ~1650 CE ± 70yrs, both SC-6 and SC-11 appear to have shifted into a different depositional environment in which most sedimentation occurred as fluvial overbank flooding and crevasse splays, or low energy, widespread fluvial sedimentation associated with the presence of a closed barrier lagoon. Closed barrier conditions result in a generally stagnant lagoon where sedimentation occurs settling of suspensions or variations on coarser deltaic wedge formation (Nichols, 1999). This sediment is typically fluvially derived as lagoon infilling after barrier closure is driven by fluvial discharge into the newly formed lagoon (Harris *et al.*, 2002). Sediments

categorized as group 1 and 5 most likely represent this depositional environment, especially the intervals deposited in the last century.

Human Impacts on Sedimentation and Sediment Accumulation Rates

Despite their complex depositional histories, both dated cores from the North Marsh platform show similar patterns of sedimentation rates changes over the last few hundred years. In both cores sedimentation rates appear to have approximately doubled over the period (decades to two centuries) prior to the 20th century lagoon modification and increased further over the course of the 20th century. The initial increase in sedimentation rate starting about 150 to 300 years ago spans the beginning of the Spanish Colonial activity through the beginning of US statehood for the region. During this period land use changes in the Scott Creek watershed may have increased sediment loading of Scott Creek and resulted in an increase in lagoon aggradation rates (ESA, 2012). However, it should be noted that sedimentation rates for these periods are highly uncertain, and that further inference would require more intensive sedimentological and historical geographic investigation.

Subsequent average sedimentation rate increases in the 20th century ranged from relatively slight (~ 20% at SC-6) to dramatic (~ 160% at SC-11, 375% at SC-9). Although these increases were coincident with hydrologic modification of lower Scott Creek, the role of Hwy. 1 bridge emplacement activities on the observed sedimentation rates cannot be definitively interpreted from the results of this study. Core chronology limitations and the massive sedimentation event during the 1955 levee breach largely prevented direct

estimation of sedimentation rates during the decades directly after the emplacement of the Hwy. 1 bridge. It is possible that other watershed disturbances including floods in 1983 and 1998, and a wildfire event in 2009 could have further influenced this apparent increase (ESA, 2012). Additionally, increases in relative sea level rise must also be contributing to long term accommodation space increases. Further investigation of changes in 20th century sediment delivery as affected by changes in land use, watershed disturbances, and hydrology would help to place these rates in context.

Furthermore, sedimentation rates over decadal scales are highly susceptible to episodic influences, particularly in the case of small mountainous river estuaries such as the Scott Creek Lagoon. Mixed fluvial/tidal marshes with variable marine connectivity and fluvial loading from a small mountainous watershed are typical of much of the California Coast. Sedimentation in these systems seems to track relative sea level rise over long (centennial to millennial) time scales because of the first order control of inundation depth on sediment delivery. However, fluvial sediment supply to these systems is highly episodic, with the vast majority of sediment flux to the ocean occurring during rare high discharge events (Farnsworth & Warrick, 2007; Gray *et al.*, 2018; Watson *et al.*, 2019). Over short (event to interdecadal) time scales, episodic sediment delivery can result in highly variable sedimentation rates (Gray *et al.*, 2016, 2018). For example, sedimentation from 1955 levee breach accounted for 36-67% of the sedimentation at the two marsh platform sites over the past 63 years.

Evidence of negative sedimentation rate feedback following rapid accretion may also be present in the North Marsh platform cores, as both exhibit subsequent

sedimentation rates that were lower than those directly preceding the breach, and then rebound over the following decades. Indeed, post 1955 sedimentation rates at SC-6 were less than pre-20th Century rates. This raises the question: was North Marsh deposition from the 1955 flood event primarily a natural expression of episodic sediment delivery in small mountainous river estuaries, or primarily the result of altered sediment trapping efficiency imposed by hydrologic modification? If the latter is the case, then not only the massive sedimentation event, but also the subsequent period of low sedimentation rates could be partially a result of hydrologic modification.

To place these sedimentation rates in a regional context, the average current rate of relative sea level (RSL) rise in the Monterey Bay region is approximately 0.15 cm yr^{-1}, which is slightly higher than the late Holocene average of 0.13 cm yr^{-1} (Reynolds & Simms, 2015). Although we do not have precise local estimates of RSL at the Scott Creek Lagoon, pre-and post-levee breach sedimentation on the North Marsh platform seems to be tracking closely with regional RSL over centennial time scales, as expected. However, it is unclear if sedimentation will continue to keep up with the projected regional RSL rise of 0.36 -1.6 cm yr^{-1} by 2060 (Revell Coastal, 2016).

Conclusions

The purpose of this study was to investigate geomorphic changes in the Scott Creek Estuary over the last two millennia. This was done to gain a better understanding of both its natural sedimentological functioning and the effects of human alteration in the last century. In the process, this approach has illustrated a way to identify sequences of channel

abandonment, and to differentiate between active main channel and abandoned channel fill in estuarine environments that are frequently inundated.

Human generated channel abandonment in the 1930s provided a unique opportunity to identify channel abandonment elsewhere in the marsh. Detailed particle size distribution partitioning and end member modeling, paired with particle size statistical bivariate domain visualization, allowed for the differentiation between two types of channel deposits. This provided evidence that the main channel was located closer to its current position (SC-11) over 2,000 years ago. Over the next two millenia, the channel migrated North to its most recent location prior to human modification. It appears to have been located closer to SC-6 between 1100-1700 CE as it migrated across the current North marsh, but there is no conclusive proof regarding the actual location of the channel, and no evidence that it occupied the site of SC-6 over the period of record. This suggests that the movement of the Scott Creek mainstem to the northerly location encountered by early European settlers was accomplished through avulsion to it's more northly location, potentially followed by slower meander migration to the north. After 1700, the North marsh appears to have reached a configuration that resembled the pre-human intervention marsh, as there was no longer direct channel connectivity depositing gravelly bedload sediments. Since then, the North Marsh platform has acted as a floodplain environment, receiving sediment during channel overtopping associated with storm events and periods of marsh inundation due to beach barrier closures, wave events, and storm surges.

Average sedimentation on the North Marsh platform ranged from 0.08 - 0.19 cm yr^{-1} over the millenium preceding human alteration of lower Scott Creek. This rate was

likely adjusted to average RSL at the marsh. A large package of sediment (12-20 cm) was likely deposited on the central portion of the North Marsh platform by the 1955 flood and levee breach event. Since then, sedimentation has occurred at rates rising from about 0.1-0.6 cm yr^{-1} over the last several decades. Although sedimentation rates in the North marsh were higher in the 20th century than during the preceding periods of European colonization and Native American land use, we are unable to conclusively state whether the emplacement of the Highway 1 bridge in 1938 affected the long term accretionary trajectory of the North Marsh over the last 80 years. Changes in trapping efficiency, a large (though episodic) fluvial sediment supply, and increases in connectivity after breaches in the north levee over the last 60 years appear to have allowed the marsh to maintain sedimentation rates equivalent to local relative sea level rise. The future accretionary trajectory of the Scott Creek Lagoon will depend upon the next phase of direct human modification, and human mediated changes in both watershed sediment loading and marine forcings.

References

Allen, J.R.L. (1965) A Review of the Origin and Characteristics of Recent Alluvial Sediments. *Sedimentology*, **5**, 89–191.

Appleby, P.G. and **Oldfield, F.** (1978) The calculation of lead-210 dates assuming a constant rate of supply of unsupported 210Pb to the sediment. *Catena*, **5**, 1–8.

Bagnold, R.A. (1966) An Approach to the Sediment Transport Problem From General Physics. Geol. Surv. Prof. Pap. 422-I

Best, T.C. and **Griggs, G.B.** (1991) A sediment budget for the Santa Cruz littoral cell, California. *From Shorel. to Abyss, SEPM Spec. Publ. No. 46*, **46**, 34–50.

Blaauw, M. and **Christen, J.A.** (2011) Flexible paleoclimate age-depth models using an autoregressive gamma process. *Bayesian Anal.*, **6**, 457–474.

Blott, S.J. and **Pye, K.** (2001) Gradistat: A Grain Size Distribution and Statistics Package for the Analysis of Unconcolidated Sediments. *Earth Surf. Process. Landforms*, **26**, 1237–1248.

Bridge, J.S., **Smith, N.D.**, **Trent, F.**, **Gabel, S.L.** and **Bernstein, P.** (1986) Sedimentology and morphology of a low-sinuosity river: Calamus River, Nebraska Sand Hills. *Sedimentology*, **33**, 851–870.

Cahoon, D.R., **Lynch, J.C.** and **Powell, A.N.** (1996) Marsh vertical accretion in a southern California estuary, U.S.A. *Estuar. Coast. Shelf Sci.*, **43**, 19–32.

Camacho-Valdez, V., **Ruiz-Luna, A.**, **Ghermandi, A.** and **Nunes, P.A.L.D.** (2013) Valuation of ecosystem services provided by coastal wetlands in northwest Mexico. *Ocean Coast. Manag.*, **78**, 1–11.

Chambers, R.L. and **Upchurch, S.B.** (1979) Multivariate analysis of sedimentary environments using grain-size frequency distributions. *J. Int. Assoc. Math. Geol.*, **11**, 27–43.

Clark, J.C. (1981) Stratigraphy, Paleontology, and Geology of the Central Santa Cruz Mountains, California Coast Ranges.

Clarke, D.W., **Boyle, J.F.**, **Chiverrell, R.C.**, **Lario, J.** and **Plater, A.J.** (2014) A sediment record of barrier estuary behaviour at the mesoscale: Interpreting high-resolution particle size analysis. *Geomorphology*, **221**, 51–68.

Costanza, R., **Pérez-Maqueo, O.**, **Martinez, M.L.**, **Sutton, P.**, **Anderson, S.J.** and **Mulder, K.** (2008) The value of coastal wetlands for hurricane protection. *Ambio*, **37**, 241–8.

Dietze, E. and **Dietze, M.** (2019) Grain-size distribution unmixing using the R package EMMAgeo. *E&G Quat. Sci. J.*, **68**, 29–46.

Dietze, E., **Hartmann, K.**, **Diekmann, B.**, **IJmker, J.**, **Lehmkuhl, F.**, **Opitz, S.**, **Stauch, G.**, **Wünnemann, B.** and **Borchers, A.** (2012) An end-member algorithm for deciphering modern detrital processes from lake sediments of Lake Donggi Cona, NE Tibetan Plateau, China. *Sediment. Geol.*, **243**–**244**, 169–180.

Environmental Science Associates (2017) Data Synthesis Memorandum for Scott Creek Lagoon and Marsh Restoration Project. 29 pp.

Environmental Science Associates (2001) Coast Dairies Property : A Land Use History. In: *Coast Dairies Long-Term Resource Protection and Use Plan: Draft Existing Conditions Report for the Coast Dairies Property, Section 1.0*, San Francisco, CA, 1–45.

Environmental Science Associates and **SWCA, E.C.** (2012) Scott Creek and Waddell Creek Bridge Replacements: Potential Physical and Biological Implications. 270 pp.

Farnsworth, K.L. and **Milliman, J.D.** (2003) Effects of climatic and anthropogenic change on small mountainous rivers: The Salinas River example. *Glob. Planet. Change*, **39**, 53–64.

Farnsworth, K.L. and **Warrick, J.A.** (2007) Sources , Dispersal , and Fate of Fine Sediment Supplied to Coastal California. *U.S. Geol. Surv. Sci. Investig. Rep. 2007-5254*, 77.

Fisk, H.N. (1947) Fine-Grained Alluvial Deposits and Their Effects on Mississippi River Activity. 82 pp.

Flemming, B.W. (2011) Geology, Morphology, and Sedimentology of Estuaries and Coasts. In: *Treatise on Estuarine and Coastal Science*, 3, 7–38.

Flemming, B.W. (2000) A revised textural classification of gravel-free muddy sediments on the basis of ternary diagrams. *Cont. Shelf Res.*, **20**, 1125–1137.

Folk, R.L. (1954) The Distinction between Grain Size and Mineral Composition in Sedimentary-Rock Nomenclature Author. *J. Geol.*, **62**, 344–359.

Folk, R.L. and **Ward, W.C.** (1957) Brazos River Bar: A Study in the Significance of Grain Size Parameters. *J. Sediment. Petrol.*, **27**, 3–26.

Friedman, G.M. (1961) Distinction between dune, beach, and river sands from their textural characteristics. *J. Sediment. Petrol.*, **31**, 514–529.

Friedman, G.M. and **Sanders, J.E.** (1978) Principles of Sedimentology. *John Wiley and Sons*, New York, 792 pp.

Grantham, T.E., **Merenlender, A.M.** and **Resh, V.H.** (2010) Climatic influences and anthropogenic stressors: An integrated framework for streamflow management in Mediterranean-climate California, U.S.A. *Freshw. Biol.*, **55**, 188–204.

Gray, A.B., **Pasternack, G.B.** and **Watson, E.B.** (2018) Estuarine abandoned channel sedimentation rates record peak fluvial discharge magnitudes. *Estuar. Coast. Shelf Sci.*, **203**, 90–99.

Gray, A.B., **Pasternack, G.B.** and **Watson, E.B.** (2010) Hydrogen peroxide treatment effects on the particle size distribution of alluvial and marsh sediments. *Holocene*, **20**, 293–301.

Gray, A.B., **Pasternack, G.B.**, **Watson, E.B.** and **Goñi, M.A.** (2016) Abandoned channel fill sequences in the tidal estuary of a small mountainous, dry-summer river. *Sedimentology*, **63**, 176–206.

Harris, P.T., **Heap, A.D.**, **Bryce, S.M.**, **Porter-Smith, R.**, **Ryan, D.A.** and **Heggie, D.T.** (2002) Classification of Australian Clastic Coastal Depositional Environments Based Upon a Quantitative Analysis of Wave, Tidal, and River Power. *J. Sediment. Res.*, **72**, 858–870.

Hemphill-Haley, E. (1996) Diatoms as an aid in identifying late-holocene tsunami deposits. *Holocene*, **6**, 439–448.

Hooke, J.M. (1995) River channel adjustment to meander cutoffs on the River Bollin and River Dane, northwest England. *Geomorphology*, **14**, 235–253.

Jones, D.A. and **Hildebrandt, W.** (1988) Archaeological Investigations at Sand Hill Bluff: Portions of Prehistoric Site CA- SCR-7, Santa Cruz County.

Krumbein, W.C. (1934) Size Frequency Distribution of Sediments. *J. Sediment. Petrol.*, **4**, 65–77.

Lario, J., **Spencer, C.**, **Plater, A.J.**, **Zazo, C.**, **Goy, J.L.** and **Dabrio, C.J.** (2002) Particle size characterisation of Holocene back-barrier sequences from North Atlantic coasts (SW Spain and SE England). *Geomorphology*, **42**, 25–42.

Lechner, A. (2009) Palaeohydrologic conditions and geomorphic processes during the postglacial in the Palatine Upper Rhine river floodplain. *Zeitschrift fur Geomorphol.*, **53**, 217–245.

Levinton, J.S. (1995) Marine Biology, 1st Ed. *Oxford University Press*, New York.

Levy, R. (1977) Costanoan. In: *Handbook of North American Indians, Vol. 8: California* (Ed. R.F. Heizer), *Smithsonian Institution*, Washington D.C.,

Martins, L.R. (1965) Significance of skewness and kurtosis in environmental interpretation. *J. Sediment. Res.*, **35**, 768–770.

McBride, R.A., **Anderson, J.B.**, **Buynevich, I. V.**, **Cleary, W.**, **Fenster, M.S.**, **FitzGerald, D.M.**, **Harris, M.S.**, **Hein, C.J.**, **Klein, A.H.F.**, **Liu, B.**, **de Menezes, J.T.**, **Pejrup, M.**, **Riggs, S.R.**, **Short, A.D.**, **Stone, G.W.**, **Wallace, D.J.** and **Wang, P.** (2013) Morphodynamics of Barrier Systems: A Synthesis. *Elsevier Ltd.*, 166–244.

Moiola, R.J. and **Weiser, D.** (1968) Textural Parameters: An Evaluation. *J. Sediment. Petrol.*, **38**, 45–53.

Mudd, S.M., **Howell, S.M.** and **Morris, J.T.** (2009) Impact of dynamic feedbacks between sedimentation, sea-level rise, and biomass production on near-surface marsh stratigraphy and carbon accumulation. *Estuar. Coast. Shelf Sci.*, **82**, 377–389.

Nelleman, C., **Corcoran, C.**, **Duarte, C.M.**, **Valdes, L.**, **De Young, C.** and **Fonseca, L.** (2009) Blue carbon. A Rapid Response Assessment.

Nichols, G. (1999) Sedimentology and Stratigraphy, Second. *Wiley-Blackwell*, 432 pp.

Nylen, B.D. (2015) Mouth Closure and Dissolved Oxygen Levels in a Small, Bar-Built Estuary : Scott Creek , California. University of California, Davis

Oczkowski, A., **Santos, E.**, **Gray, A.**, **Miller, K.**, **Huertas, E.**, **Hanson, A.**, **Martin, R.**, **Watson, E.B.** and **Wigand, C.** (2019) Tracking the Dynamic Ecological History of a Tropical Urban Estuary as it Responds to Human Pressures.

Osterback, A.M.K., **Kern, C.H.**, **Kanawi, E.A.**, **Perez, J.M.** and **Kiernan, J.D.** (2018) The effects of early sandbar formation on the abundance and ecology of coho salmon (Oncorhynchus kisutch) and steelhead trout (Oncorhynchus mykiss) in a central California coastal lagoon. *Can. J. Fish. Aquat. Sci.*, **75**, 2184–2197.

Pejrup, M. (1988) The triangular diagram used for classification of estuarine sediments: a new approach. In: *Tide-Influenced Sedimentary Environments and Facies* (Ed. P.L. de Boer), *D. Reidel Publishing Company*, 289–300.

Perg, L.A., **Anderson, R.S.** and **Finkel, R.C.** (2003) Use of cosmogenic radionuclides as a sediment tracer in the Santa Cruz Littoral cell, California, United States. *Geology*, **31**, 299–302.

Poizot, E., **Méar, Y.** and **Biscara, L.** (2008) Sediment Trend Analysis through the variation of granulometric parameters: A review of theories and applications. *Earth-Science Rev.*, **86**, 15–41.

Rafter, T.A. and **Fergusson, G.J.** (1957) "Atom Bomb Effect" - Recent Increase of Carbon-14 Content of the Atmosphere and Biosphere. *Science (80-.).*, **126**, 557–558.

Reimer, P.J., **Bard, E.**, **Bayliss, A.**, **Beck, J.W.**, **Blackwell, P.G.**, **Ramsey, C.B.**, **Buck, C.E.**, **Cheng, H.**, **Edwards, R.L.**, **Friedrich, M.**, **Grootes, P.M.**, **Guilderson, T.P.**, **Haflidason, H.**, **Hajdas, I.**, **Hatté, C.**, **Heaton, T.J.**, **Hoffmann, D.L.**, **Hogg, A.G.**, **Hughen, K.A.**, **Kaiser, K.F.**, **Kromer, B.**, **Manning, S.W.**, **Niu, M.**, **Reimer, R.W.**, **Richards, D.A.**, **Scott, E.M.**, **Southon, J.R.**, **Staff, R.A.**, **Turney, C.S.M.** and **van der Plicht, J.** (2013) IntCal13 and Marine13 Radiocarbon Age Calibration Curves 0–50,000 Years cal BP. *Radiocarbon*, **55**, 1869–1887.

Revell Coastal LLC (2016) 2016 City of Monterey Final Sea Level Rise and Vulnerability Analyses, Existing Conditions and Issues Report. 1–67 pp.

Reynolds, L.C. and **Simms, A.R.** (2015) Late Quaternary relative sea level in Southern California and Monterey Bay. *Quat. Sci. Rev.*, **126**, 57–66.

Sahu, B.K. (1964) Depositional Mechanisms from the Size Analysis of Clastic Sediments. *J. Sediment. Petrol.*, **34**, 73–83.

Smith, J.J. (1990) The effects of sandbar formation and inflows on aquatic habitat and fish utilization in Pescadero, San Gregorio, Waddell, and Pomponio Creek estuary/lagoon systems, 1985-1989. *Department of Biological Sciences, San Jose State University*, San Jose, CA.

Stewart, H.B. (1958) Sedimentary reflections on depositional environments in San Miguel Lagoon, Baja California, Mexico. *Bull. Am. Assoc. Pet. Geol.*, **42**, 2567–2618.

Szczuciński, W., **Kokociński, M.**, **Rzeszewski, M.**, **Chagué-Goff, C.**, **Cachão, M.**, **Goto, K.** and **Sugawara, D.** (2012) Sediment sources and sedimentation processes of 2011 Tohoku-oki tsunami deposits on the Sendai Plain, Japan - Insights from diatoms, nannoliths and grain size distribution. *Sediment. Geol.*, **282**, 40–56.

Tanner, W.F. (1991) Application of suite statistics to stratigraphy and sea-level changes. In: *Principles, Methods, and Applications of Particle Size Analysis* (Ed. J.P.M. Syvitski), *Cambridge University Press*, Cambridge, 283–292.

Tanner, W.F. (1995) Environmental clastic granulometry. In: *Florida Geological Survey*, Special Pu, 1–162.

Toonen, W.H.J., **Kleinhans, M.G.** and **Cohen, K.M.** (2012) Sedimentary architecture of abandoned channel fills. *Earth Surf. Process. Landforms*, **37**, 459–472.

Valia, H.S. and **Cameron, B.** (1977) Skewness as a Paleoenvironmental Indicator. *J. Sediment. Petrol.*, **47**, 784–793.

Visher, G.S. (1969) Grain Size Distributions and Depositional Processes. *J. Sediment. Petrol.*, **39**, 1074–1106.

Waters, C.N., **Syvitski, J.P.M.**, **Gałuszka, A.**, **Hancock, G.J.**, **Zalasiewicz, J.**, **Cearreta, A.**, **Grinevald, J.**, **Jeandel, C.**, **McNeill, J.R.**, **Summerhayes, C.** and **Barnosky, A.** (2015) Can nuclear weapons fallout mark the beginning of the Anthropocene Epoch. *Bull. At. Sci.*, **71**, 46–57.

Watson, E.B., **Gray, A.B.**, **Pasternack, G.B.** and **Woolfolk, A.M.** (2019) Retention of alluvial sediment in the tidal delta of a river draining a small, mountainous coastal watershed. *Cont. Shelf Res.*, **182**, 1–11.

Watson, E.B., **Pasternack, G.B.**, **Gray, A.B.**, **Goñi, M.** and **Woolfolk, A.M.** (2013) Particle size characterization of historic sediment deposition from a closed estuarine lagoon, Central California. *Estuar. Coast. Shelf Sci.*, **126**, 23–33.

Yu, L. and **Oldfield, F.** (1989) A multivariate mixing model for identifying sediment source from magnetic measurements. *Quat. Res.*, **32**, 168–181.